The Effect of Endografts on the Propagation of Aortic Dissection: A Fluid-Structure Interaction (FSI) Finite-Element Model of Flow through the Descending Thoracic Aorta

A THESIS
SUBMITTED TO THE FACULTY OF THE GRADUATE SCHOOL
OF THE UNIVERSITY OF MINNESOTA
BY

Ankurita Datta

IN PARTIAL FULFILLMENT OF THE REQUIREMENTS
FOR THE DEGREE OF
MASTER OF SCIENCE

Dr. Victor H. Barocas

July, 2017

Acknowledgements

I would like to thank my advisor, Professor Victor Barocas, for his academic guidance, patience, and support.

I express my greatest appreciation to my thesis committee members Dr. Filippo Coletti and Dr. Rumi Faizer for their passion and support, and to Dr. Omid Amili for always willing to help.

A special thank you to Dr. Vineet Rakesh for his advice and encouragement of the project. His guidance with fluid structure interaction simulations and COMSOL was invaluable.

I would like to acknowledge the Minnesota Supercomputing Institute (MSI) at the University of Minnesota for providing the computational resources and personnel that allowed for the results obtained in this thesis. (URL:http://www.msi.umn.edu)

Finally, I would like to send my endless gratitude to my family and friends especially Steph, my sister Amita, and my dad. Thank you for believing in me; I am so lucky to have you.

Dedication

For my father.

Thank you for your good humor and unwavering love.

Abstract

Tears in the lining of the aorta are termed aortic dissections. Aortic dissections affect 12,000 new patients per year in the US and are associated with significant morbidity and mortality. The primary management method is an invasive and difficult surgery to replace the dissected portion of the aorta with a synthetic graft. However, recent randomized trials on the use of minimally invasive stent-grafts to treat aortic dissection have proved promising.

Though the precise etiology of aortic dissections is unclear, the underlying pathophysiology may be related to hypertension induced injury in an aorta that has lost compliance due to aging. Though stent-grafts can effectively protect the initial location of the dissection, stent-grafts are essentially stiff tubes and after implantation, residual portions of the native aorta proximal and distal to the stent-graft are needed to dissipate systolic pressure. These regions of the native aorta proximal to the stent-graft required to limit pressure differences are exposed to larger stresses thus increasing the potential of aortic tearing. Stent-graft-induced new entry, SINE, has been recorded in 30% of patients treated with a stent-graft for aortic dissection.

It is hypothesized that the stiffness of the stent-graft itself may exacerbate pressure in the proximal and distal native aorta and may be responsible for stent-graft induced new tears. A mathematical lumped parameter model and computational finite-element model were developed to evaluate this.

The lumped parameter model uses electrical analogs for blood flow and compliances of the native aorta and stent-graft respectively. The mathematical model predicts an increased peak pressure for a stiff stent-graft as compared to a compliant stent-graft. Additionally, the mathematical model predicts an increase in peak pressure with an increase in stent-graft length. Motivated by the need to incorporate more anatomically accurate material properties and capture complexities of the flow field, a three-dimensional computational model of the flow through the descending thoracic aorta

and stent-graft was developed. For an aortic dissection patient treated with a stiff stent-graft, the computational model predicts a peak cardiac cycle pressure of 190 mmHg, as compared to the predicted pressure of 176 mmHg for an aortic dissection patient treated with a compliant stent-graft. The model suggests that the increase in stent-graft length increases peak pressure during the length of the cardiac cycle, but a change in stent-graft modulus and stent-graft position does not affect the peak pressure during the length of the cardiac cycle.

The modeling developed in this thesis confirms that the stiffness of the stent-grafts used to treat aortic dissection affects pressures in the proximal native aorta and could contribute to the formation of stent-graft induced new entry. This information is critical to the development of future stent-grafts to treat aortic dissection.

Contents

List of Tables

List of Figures

Chapter 1

Introduction

The cardiovascular system consists of the heart and blood vessels and is responsible for delivering oxygen and nutrients to the tissues and organs of the body. The heart acts as a pump and generates high-pressure blood, which is then circulated throughout the vasculature. The cardiovascular system is divided into two circuits: the pulmonary circulation and systemic circulation. The pulmonary circulation carries deoxygenated blood to the lungs from the heart, and returns oxygenated blood back to the heart from the lungs. The systemic circulation carries oxygenated blood to the body from the heart, and returns deoxygenated blood back to the heart from the rest of the body.

Arteries are the major blood vessels of the systemic circulation that carry oxygenated blood away from the heart. Oxygen and nutrients are delivered to tissues of the body through diffusion through the arterial wall. In order to enhance nutrient transport, arteries divide into smaller radii arteries, arterioles, and capillaries to increase the available surface area for transport. Capillaries are the smallest vessels in the cardiovascular system and are the site of oxygen and nutrient exchange. After the capillaries, deoxygenated blood returns to the heart via a system of veins and venules to be reoxygenated.

1.1 Background

In the scope of this project, the major artery discussed is the aorta. The aorta is the first artery that blood enters upon ejection from the heart and is the largest artery of the body. It is most commonly divided into four major sections: the ascending aorta, aortic arch, descending aorta, and abdominal aorta, the locations of which can be seen in Figure 1.1. The aorta is composed of a thick layer of smooth muscle and three distinct layers of connective tissue and elastic fibers: the intima (inner layer), media, and adventitia (outer layer) [9].

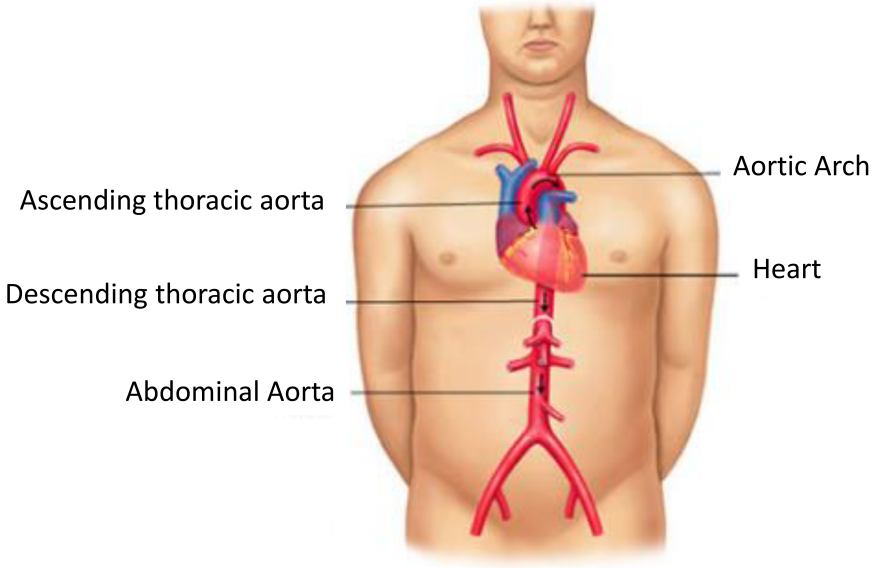

Figure 1.1: The aorta is the major artery of the systemic system. From Sayed, 2017 [2].

Blood flow through the aorta is controlled by the contraction and relaxation of the ventricles. The contraction of the ventricles, termed cardiac systole, creates an increase in pressure, which drives blood through the aorta and remaining vasculature. Blood flows through the vasculature from high to low pressure, mediated by the resistance of the blood vessels. As the radius of the arteries, arterioles, and capillaries decrease, the elastin content of blood vessels decreases [20]. This loss of elasticity creates the resistance to blood flow within the smaller arteries and capillaries. The aorta, the largest

artery of the cardiovascular system, controls the flow of blood into the circulation by mechanically stretching or contracting.

Diseases of the cardiovascular system can lead to abnormalities of the aortic wall and significantly alter the ability of the aorta to control the flow of blood into the circulation. Common abnormalities include aneurysms, which are enlargements of the aorta, and aortic dissections, which are tearings in the inner lining of the aorta.

An aortic dissection generally occurs in a more brittle area of the aortic wall, where chronic high blood pressure induces stresses on the aorta, making it highly susceptible to tearing. This tearing allows blood to enter the inner layers of the aortic wall, forming an artificial channel for blood flow called the "false lumen", and can cause multiple challenges (Figure 1.2) [9]. A false lumen can prevent blood from reaching other vital organs, can block flow within the true aorta lumen, and most fatally can lead to rupture or the formation of an aneurysm.

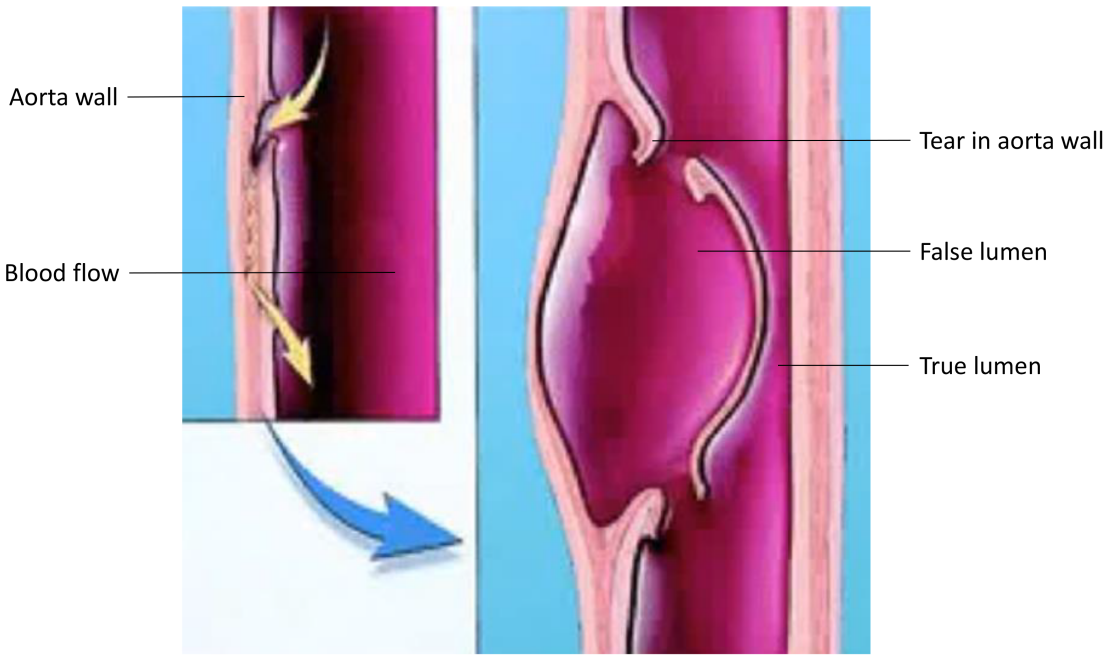

Figure 1.2: An aortic dissection is a tearing within the inner wall of the aorta. From AlKhaderi, 2016 [1].

Aortic dissections are divided into two groups according to the part of the aorta affected. Tears in the ascending aorta are called Type A dissections, and tears that do not involve the ascending aorta are called Type B dissections [16]. Type A and B aortic dissections combined affect approximately 12,000 new patients per year in the US, and are associated with significant morbidity and mortality [15]. The primary management method is surgical treatment to replace the dissected portion of the aorta with a synthetic graft [9]. This is a very invasive and difficult procedure and it requires aggressive hypertension medication to control the blood pressure differences between cardiac systole and diastole to prevent the potential formation of new tears [16]. However, studies have shown that blood pressure management is not always protective. For survivors of Type B aortic dissection, there is a reported 20-40% aorta related mortality within 5 years for patients treated with the best medical treatment [3].

1.2 Motivation

Recent randomized trials on the use of stent-grafts to treat aortic dissection have been promising. A stent-graft is placed within the diseased portion of the native aorta and creates a barrier between blood flow and the native aorta. One-year results from the recent ADSORB (Acute Dissection Stent-graft OR Best Medical Treatment) trial indicate that the placement of a stent-graft in patients with aortic dissection induces thrombosis within the false lumen and returns the normal flow of blood to the true lumen of the aorta [3]. However, segmental coverage of the dissected aorta with a stent-graft only masks the diseased portion of the vessel from fluid flow and does not heal the underlying pathology of the aortic wall that led to the initial separation of the aortic wall layers.

The high elastin content of a healthy descending thoracic aorta allows for the absorption and redistribution of the large bolus of blood ejected by the heart during cardiac systole. As mentioned previously, a healthy aorta stretches and contracts to control the flow of blood into the vasculature. Stent-grafts used for the treatment of aortic dissection were originally designed for the treatment of aortic aneurysms and are relatively

stiff in the circumferential direction to prevent expansion of the aorta and blood flow into the aneurysmal space. While these stiff stent-grafts are FDA approved for the treatment of acute aortic dissection, they do not provide the circumferential expandability of the native aorta, necessary for the treatment of aortic dissection. Though the stiff stent-grafts may protect the initial location of the dissection, it is hypothesized that larger regions of the native aorta proximal and distal to the implantation of the stiff stent-graft are required to limit the pressure differences during the cardiac cycle. These larger regions are exposed to higher pressures and thus larger stresses, increasing the potential of tearing. Stent-graft induced new tears in locations adjacent to the initial implantation of the stiff stent-graft, termed SINE (Stent-graft induced new entry), have been recorded in 30% of patients treated with a stent-graft for aortic dissection [17].

1.3 Hypothesis and Objectives

It is hypothesized that an increase in the compliance of the stent-graft such that it is able to mimic properties of the normal aorta, could reduce pressures proximal to the stent-graft, thus limiting the risk of SINE dissections, and potentially preventing the necessity of aggressive hypertension management.

The main objective of this work is to investigate whether one fundamental cause of SINE dissections is an increase in internal blood pressure with the incorporation of a stiff stent-graft into the native descending thoracic aorta by using:

- A lumped parameter model and
- Fluid-structure interaction (FSI) finite-element simulations.

Chapter 2

Methods

2.1 Lumped Parameter Model

A windkessel is an air chamber used in fire engines; water is pumped into the air chamber which expands or contracts to allow for the constant rate of water flow through the spout (Figure 2.1) [23]. The biological windkessel model similarly uses this basic windkessel to describe flow within the arterial system; the walls of the aorta act as the windkessel to ensure the steady flow of blood into the peripheral vasculature (Figure 2.1). As blood pressure rises during cardiac systole, the elastic expansion of the aorta stores blood flow, and during the low pressure stroke of cardiac diastole, the elastic nature of the aorta squeezes blood through the rest of the vasculature, smoothing out the pressure pulses of the cardiac cycle (Figure 2.1) [18]. The blood pressure waveform generated by the heart is assumed to be transmitted instantaneously through the aorta. The smaller arteries, arterioles, and capillaries act as high-resistance vessels to allow for a nearly constant flow of blood into the peripheral organs and tissues [11].

The fluid flow through the biological simplification of the arterial system is analyzed mathematically by translating the windkessel model into an electrical circuit model analog. In fluid mechanics, the pressure P, drives fluid flow at a flow rate, Q (Equation 2.1). As the resistance, R_{es}, to flow rate is increased, the volume flow rate decreases proportionately. In an electrical analog, the voltage, V, drives the flow of

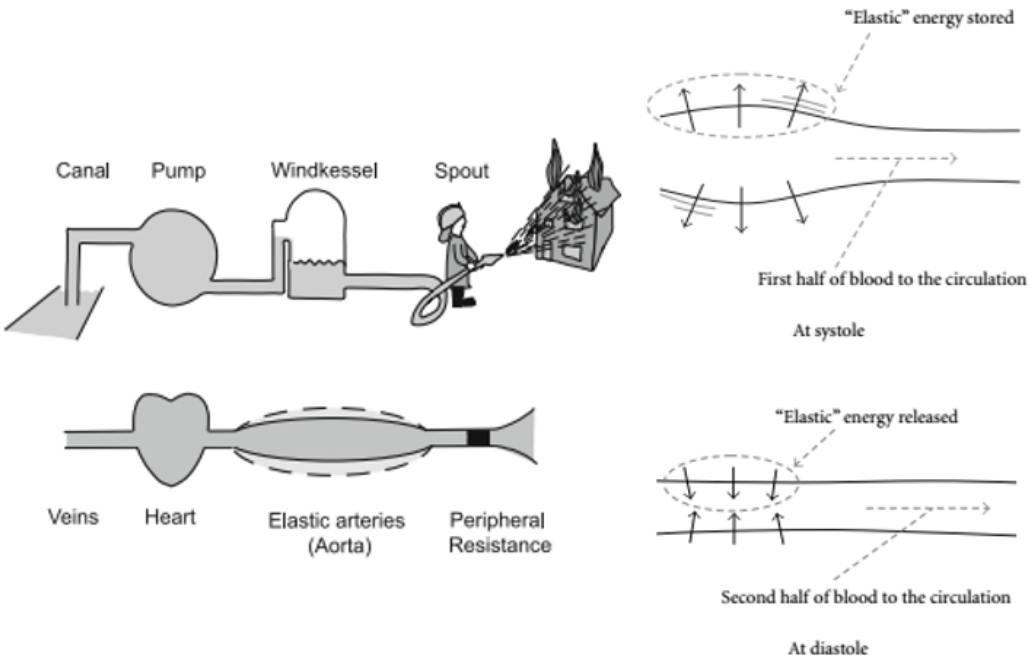

Figure 2.1: The windkessel model. (Left) The windkessel used in fire engines and the biological windkessel used to describe flow within the biological simplification of the arterial system. From Westerhof et al., 2009 [23]. (Right) The elastic expansion of the aorta stores energy during cardiac systole and releases energy during cardiac diastole. From Roy et al., 2012 [18].

charge (electrons), I (Equation 2.2). As the resistance, R_{es}, to flow rate is increased, the flow of charge decreases proportionately.

Fluid

$$\Delta P = QR_{es} \tag{2.1}$$

Electrical

$$\Delta V = IR_{es} \tag{2.2}$$

The three-element windkessel model simplifies each part of the arterial system to RC circuit elements. As blood leaves the heart, it first enters the proximal aorta. The proximal aorta is modeled as an impedance, Z, in the electrical analog. The characteristic impedance is interpreted as the incorporation of wave travel into the arterial system; characteristic impedance equals wave speed times blood density divided by aortic cross-sectional area [11]. The impedance element acts to absorb high frequency pulse waves. Then, blood travels to minor arteries, arterioles and capillaries, which are modeled as one resistance, R. Once blood is pumped out of the heart and past the impedance of the proximal aorta, it can either be stored in a region of the expanded aorta, or travel down into the resistance of the arteries, arterioles, and capillaries; this induces a parallel effect of fluid flow into the circulation. The storage of volume in the elastically compliant aorta is analogous to the storage of charge in a capacitor and is modeled as such, C. The electrical analog of the arterial system is shown in (Figure 2.2).

Using basic circuit theory, the pressure at the proximal aorta, can be calculated from the flow rate of blood through the aorta (Equation 2.3):

$$\frac{dP(t)}{dt} = \left(1 + \frac{Z}{R}\right)\frac{Q(t)}{C} + Z\frac{dQ(t)}{dt} - \frac{P(t)}{CR} \tag{2.3}$$

where P, is the inlet aorta pressure, Z is the impedance of the proximal aorta, R_{tot} is the total peripheral resistance, Q is the flow rate of blood into the aorta, and C is the compliance of the aorta.

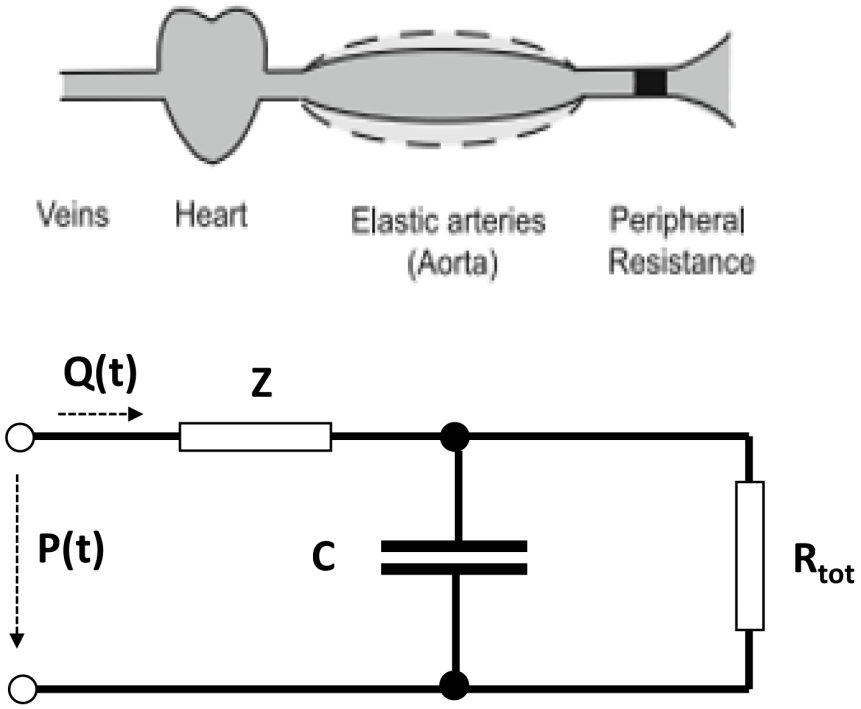

Figure 2.2: (Top) Windkessel model used to describe flow within a biological simplification of the arterial system. From Westerhof et al., 2009 [23] (Bottom) Electrical analog of the three-element windkessel model.

In order to test whether the inlet aortic pressures are increased when a stiff stent-graft is placed within a compliant native aorta, the electrical analog of the arterial system shown in Figure 2.2 is modified to include three capacitors in series (Figure 2.3). The three capacitors represent the native aorta, stiff stent-graft, and native aorta, respectively.

Using basic circuit theory for capacitors in series (Equation 2.5) the equation for the pressure at the inlet of the aorta as a function of time is derived (Equation 2.4):

$$\frac{dP(t)}{dt} = \left(1 + \frac{Z}{R}\right)\frac{Q(t)}{C_s} + Z\frac{dQ(t)}{dt} - \frac{P(t)}{C_s R} \tag{2.4}$$

where P, is the inlet aorta pressure, Z is the impedance of the proximal aorta, R_{tot} is the total peripheral resistance, Q is the flow rate of blood into the aorta, and C_s is the effective compliance of the native aorta and stent-graft in series defined by,

$$\frac{1}{C_s} = \frac{1}{C_1} + \frac{1}{C_2} + \frac{1}{C_3} \tag{2.5}$$

where C_1, C_2, and C_3 are the compliances of the native aorta, stent-graft, and native aorta respectively. Physiological values for the flow rate of blood into the aorta were obtained from Kousera et al (Appendix A.2) [12].

Constants for circuit elements C, Z, and R_{tot} were obtained from the data of Kind et al. for normotensive and hypertensive patients [10]. The aorta of a hypertensive patient is more stiff [6] and thus, compliance values for the hypertensive patient are used to describe the stiff stent-graft and slightly modified compliance values for the normotensive patient are used to describe the older patient with a healthy aorta (Appendix A.3).

2.1.1 Limitations of the Lumped Parameter Model

The windkessel model is unable to capture details of the flow field characteristics of blood through the descending thoracic aorta. In addition, the windkessel model cannot account for anatomically accurate aortic material properties. It assumes that the compliance of the aorta is constant during the cardiac cycle, whereas biological tissues have a non-linear stress-strain curve.

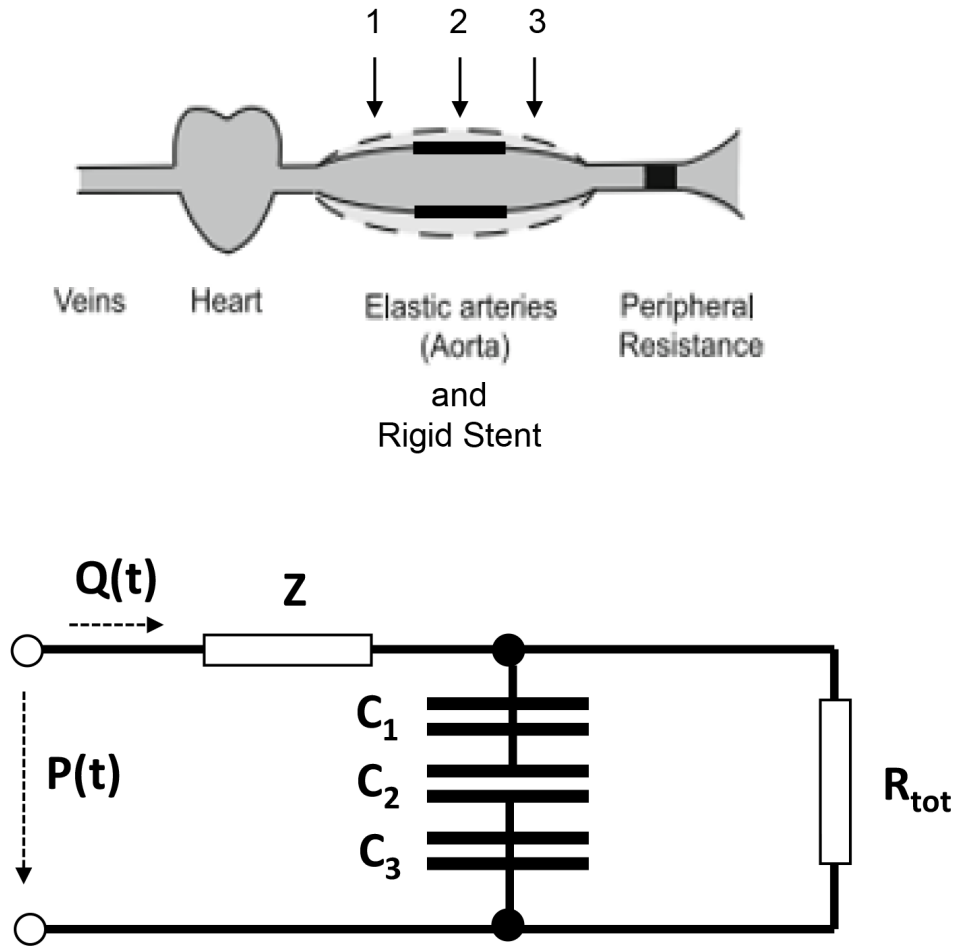

Figure 2.3: (Top) Modified windkessel model with (1) native compliant aorta, (2) stiff stent-graft, and (3) native compliant aorta. Modified from Westerhof et al. [23]. (Bottom) Electrical analog with three capacitors in series, with (1) native compliant aorta, (2) stiff stent-graft, and (3) native compliant aorta.

2.2 Fluid-Structure Interaction Finite-Element Model

A simplified finite element model of the aorta stent-graft system was developed to address some of the limitations of the windkessel model.

2.2.1 Model Schematic

A simple three-dimensional model was developed using COMSOL 5.2a to understand the internal pressure change with the interaction of blood with a compliant aortic material and a stiff stent-graft (Figure 2.4).

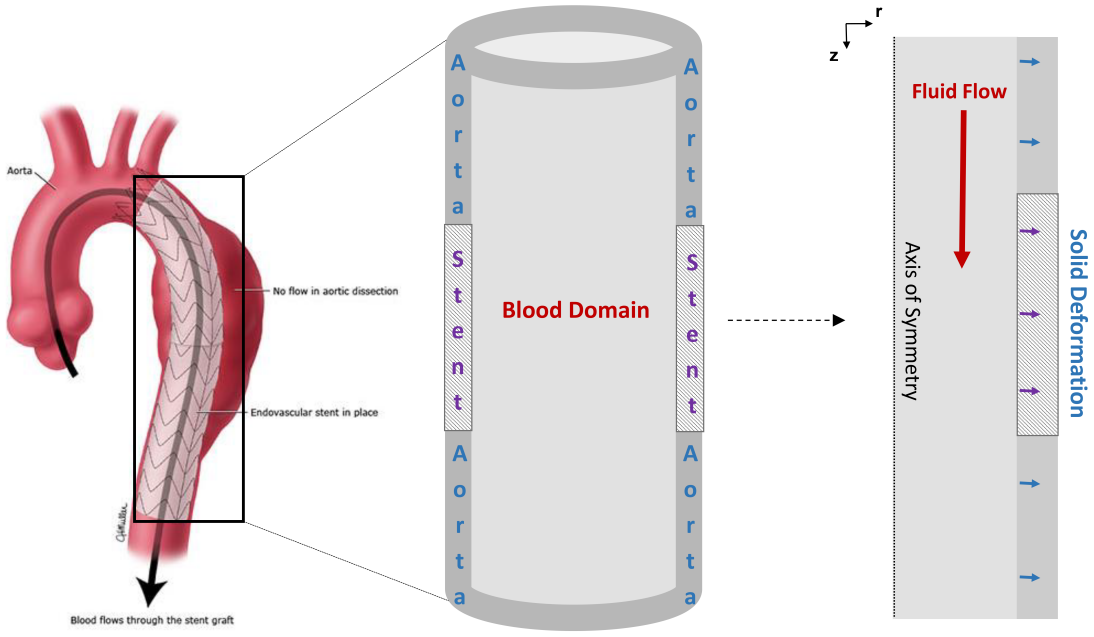

Figure 2.4: Simplified 3D COMSOL model. (Left) Physiological aorta diagram with stent-graft [2]. (Middle) Schematic of COMSOL computational domain. (Right) Axisymmetric schematic of COMSOL computational domain.

The geometry was simplified drastically to that of a cylindrical tube. The computational model domain was divided into 3 distinct regions: (1) the inner lumen of the descending aorta, (2) the wall of the descending thoracic aorta and (3) the stent-graft.

The computational model simulated the fluid flow in the inner lumen of the descending thoracic aorta and resulting deformation of the aortic wall and stiff stent-graft.

In order to ensure a more significant deformation in the aortic and stent-graft solid materials, an additional region of fluid flow was added at the outlet of the descending thoracic aorta (Figure 2.5). This additional region accounts for the resistance of the peripheral vasculature and induces a more anatomically accurate pressure distribution within the descending thoracic aorta.

2.2.2 Governing Equations

Solid Mechanics

Stent-graft The stiff stent-graft is modeled as a nearly incompressible, isotropic, linear elastic material. The density of the stent-graft was set to ρ_{stent} and the Poisson's ratio was set to ν_{stent} [18]. The deformation of the stent-graft was modeled using the equation of motion (Equation 2.6) and Hooke's Law constitutive model for linear elastic materials (Equation 2.7):

$$\nabla \cdot \sigma_{stent} = \rho \frac{\partial^2 u_{stent}}{\partial t^2} \tag{2.6}$$

$$\sigma_{stent} = E_{stent} \epsilon_{stent} \tag{2.7}$$

where σ_{stent} is the Cauchy stress in the stent-graft, u_{stent} is the stent-graft wall displacement, E_{stent} is the Young's Modulus of the stent-graft, and ϵ_{stent} is the linear strain of the stent-graft. The stent-graft thickness was set to be equal to the thickness of the aortic wall, h_{aorta}. Parameters and dimensions for the stent-graft model are displayed in Appendix A.4.

Aorta To incorporate the nonlinear interactions between blood flow and aorta, the aorta is modeled as a nearly incompressible, hyperplastic material with a specified strain energy density function, W, and the equation of motion (Equation 2.8):

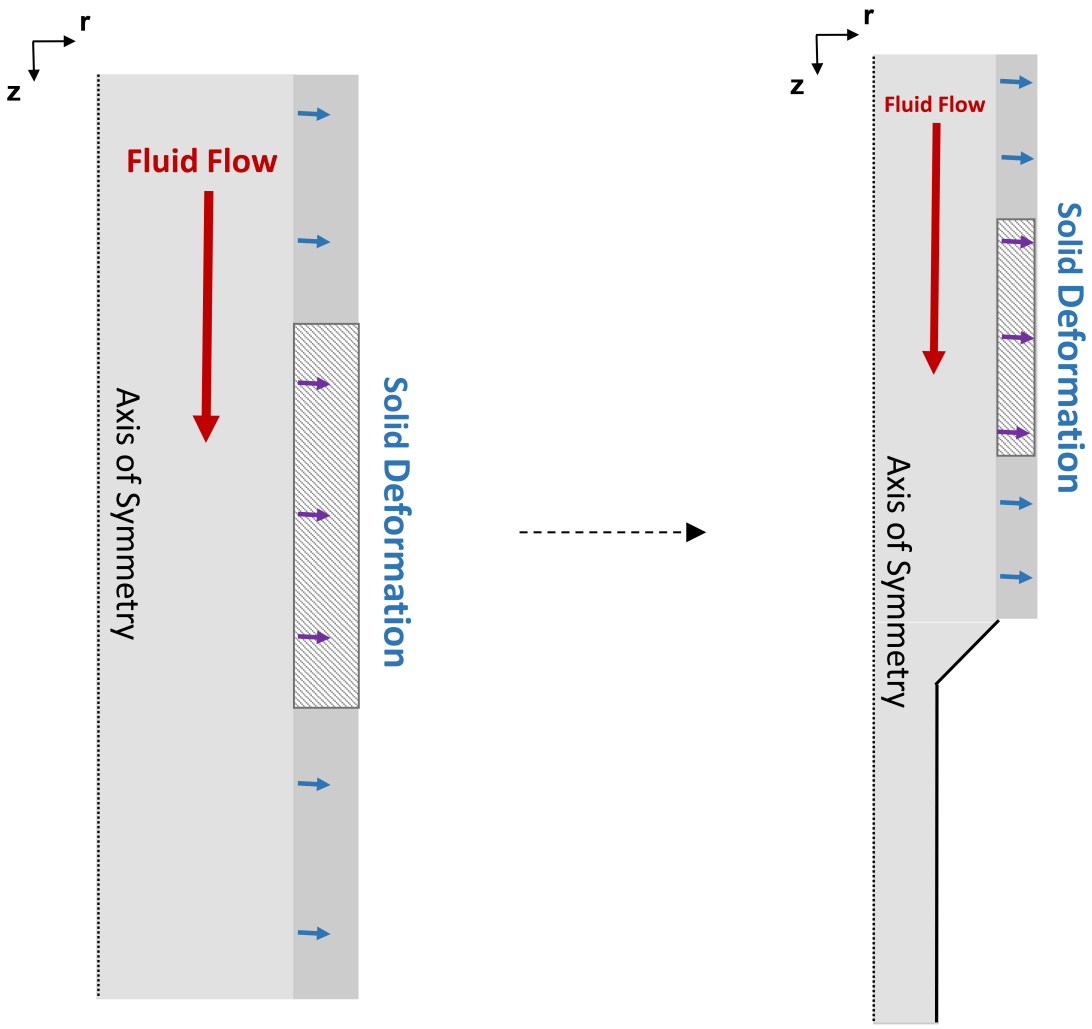

Figure 2.5: Modified 3D COMSOL model. (Left) Axisymmetric schematic of COMSOL computational domain. (Right) Modified axisymmetric schematic of COMSOL computational domain, with additional region to account for the resistance of the peripheral vasculature.

$$\nabla \cdot \sigma_{aorta} = \rho \frac{\partial^2 u_{aorta}}{\partial t^2} \tag{2.8}$$

where σ_{aorta} is the Cauchy stress in the aorta and u_{aorta} is the aortic wall displacement. The density of the aorta was set to ρ_{aorta} and the Poisson's ratio was set to ν_{aorta} [10]. The aortic wall thickness was set to a uniform thickness, h_{aorta} (Appendix 4).

In order to determine an appropriate constitutive model to accurately represent the effect of aging on mechanical properties, experimental data obtained from Groenink et al., who studied the influence of aging on the stress-strain behavior in the human descending thoracic aorta [6], were used. In Groenink's experiment, 2mm-long aortic segments from 14 patients aged 8-59 are exposed to increasing internal pressure loads.

To incorporate the change in mechanical behavior with aging, the physiological data was fit to different constitutive models to determine the model that would most accurately fit the data. The Ogden fit was used to describe the deformation of the aorta in an older patient (Figure 2.6).

The two-term incompressible Ogden model has strain energy density function, W_{O2} (Equation 2.9):

$$W_{O2} = \frac{\mu_1}{\alpha_1}\left(\lambda_1^{\alpha_1} + \lambda_2^{\alpha_1} + \lambda_3^{\alpha_1}\right) + \frac{\mu_2}{\alpha_2}\left(\lambda_1^{\alpha_2} + \lambda_2^{\alpha_2} + \lambda_3^{\alpha_2}\right) \tag{2.9}$$

where μ_1, μ_2, α_1, and α_2 are model fitting parameters and λ_1, λ_2, and λ_3 are the principal stretches in the 1, 2, and 3 directions respectively. For an incompressible material undergoing uniaxial deformation, the stress-strain relationship for a two-term Ogden model is Equation 2.10:

$$\sigma_{O2} = \mu_1\left(\lambda_1^{\alpha_1} - \lambda_1^{-0.5\alpha_1}\right) + \mu_2\left(\lambda_1^{\alpha_2} - \lambda_1^{-0.5\alpha_2}\right) \tag{2.10}$$

The stress-strain relationship for the hyperelastic aorta is implemented into COMSOL (Equation 2.11):

$$\sigma = 144.87\left(\lambda_1^{19.353} - \lambda_1^{-0.5*19.353}\right) + 9.69E6\left(\lambda_1^{0.0457} - \lambda_1^{-0.5*0.0457}\right) \tag{2.11}$$

Fluid Mechanics

Blood is modeled as a Newtonian fluid using the transient incompressible momentum (Equation 2.12) and continuity (Equation 2.13) equations:

$$\rho_{blood}\frac{\partial \vec{v}}{\partial t} + \rho_{blood}\left(\vec{v}\cdot\nabla\right)\vec{v} = -\nabla P + \mu_{blood}\nabla^2\vec{v} \quad (2.12)$$

$$\nabla\cdot\vec{v} = 0 \quad (2.13)$$

where $\vec{v}$ is the velocity vector, t is time, P is pressure, ρ_{blood} is the fluid density, and μ_{blood} is the viscosity (Appendix A.4) [14]. Gravity is assumed to be negligible.

The flow has a maximum Reynolds number around 6,000 and enters the turbulent regime. However, to simplify the computation, this study models blood flow in the laminar regime. It is assumed that turbulence models would add to the computational time without enhancing our understanding of the solution. This can be incorporated into the solution in the future if deemed necessary.

Fluid-Structure Interaction

At the interface between the blood and solid domain there is a fluid-structure interaction boundary. At this boundary, the displacement in the blood domain equals the displacement in the aortic and stent-graft solid domains (Equation 2.14) and stresses in the blood domain are translated directly to the aorta and stent-graft domains (Equation 2.15).

$$u_{blood} = u_{solid} \quad (2.14)$$

$$\sigma_{blood}\cdot n = \sigma_{solid}\cdot n \quad (2.15)$$

where u_{blood} is the displacement in the blood domain, u_{solid} is the displacement in the aortic and stent-graft solid domains, σ_{blood} is the stress in the blood domain, and σ_{solid} is the stress in the aorta and stent-graft domains.

2.2.3 Boundary Conditions

Solid domain

Axial deformation of the descending thoracic aorta is assumed to be negligible and therefore the geometry is constrained in the axial direction at the inlet and outlet. According to Humphrey, blood pressure induced axial extensions tend to be very small (1%) in the descending thoracic aorta [8]. In the pulmonary artery and ascending aorta the axial deformations can be much larger (∼5-11%) [15].

The geometry is free to move in the radial and circumferential directions at all locations (Equation 2.16):

$$n \cdot u_{solid} = 0 \tag{2.16}$$

where u_{solid} is the radial and circumferential displacement of the aorta and stent-graft solid domains.

The tissue surrounding the aorta has a resistive effect on the movement of the aortic wall. This resistance is incorporated into the model by applying a spring boundary condition. A spring stiffness of 75 mmHg/mm was used, indicating that if 75 mmHg of pressure is applied to the aorta wall, it will be displaced by 1mm [14]. The spring stiffness is converted to a spring stiffness per unit area, k_{tissue}, and is used throughout the simulation (Equation 2.17):

$$n \cdot u_{solid} = -k_{tissue} \left(u_{aorta} - u_{aorta,0}\right) \tag{2.17}$$

where $u_{aorta,0}$ represents the initial location of the aorta wall. This represents an approximation of the resistive effect of the surrounding tissues and organs on the aorta, and helps induce a more significant deformation within the solid.

Fluid domain

Blood ejected from the heart travels up the aortic arch, past the ascending thoracic aorta and down the descending thoracic aorta. It is assumed that the flow is fully developed once it reaches the descending aorta. Cardiac systole and diastole induce a pulsatile

flow in the aorta. The inlet of the fluid domain was set to a pulsating physiological flow rate (Appendix A.2).

The pressure at the outlet of the fluid domain was set to the minimum physiological pressure during the cardiac cycle, P_{min}.

The boundary conditions for the fluid and solid domains are summarized in Figure 2.7 and Appendix A.4.

2.2.4 Initial Conditions

The initial conditions in the blood domain were set to zero velocity and pressure. The initial conditions in the aorta and stent-graft domain were set to zero displacement and zero stress.

2.2.5 Mesh

In order to obtain a computational solution of the pressure at the inlet of the descending thoracic aorta, the geometry needs to be divided into smaller regions. These smaller regions are known as elements and are defined by a set of points called nodes. The finite element method reduces the governing equations into an algebraic approximation and solves this algebraic approximation at each of the nodes. The solution at regions between the nodes are interpolated based on a scheme that is built into the solution process. This collection of elements is called a mesh.

A mapped mesh with a finer mesh density near the boundary of the fluid is used to capture the steep velocity gradient at the fluid structure interface (Figure 2.8).

According to Hansen and Degroote, FSI simulations differ from other numerical problems in that decreasing the time step may cause the solution to become unstable and produce oscillations [4, 7]. Mathematical details of the cause of oscillations are omitted here as they are outside the scope of this thesis, but the reader is encouraged to read *Development Algorithms for the Partitioned Simulation of Strongly Coupled Fluid-Structure Interaction Problems* by J. Degroote [4]. Multiple simulations were run, and

the optimum time step for the older patient without a stent-graft, older patient with a stiff stent-graft, and older patient with a compliant stent-graft were chosen (Table 2.1).

Table 2.1: Time step tests to find convergence.

Simulation	Number of Mesh Elements	Δt	Convergence?
Older patient without stent-graft	12,861	free	Yes
		0.01	No
Older patient with stiff stent-graft	12,861	free	Yes
		0.01	Yes
		0.001	No
Older patient with compliant stent-graft	12,861	free	Yes
		0.01	No

Once temporal resolution was obtained, the peak inlet pressure over the cardiac cycle was obtained for different mesh densities and plotted as a function of number of elements in the mesh (Figure 2.9). A mesh convergence analysis refers to the process of solving multiple simulations with an increasing number of elements to determine the least number of elements where the solution does not change. A larger number of elements increases computational time, and thus the least number of elements that can produce an accurate solution is preferred.

The peak inlet pressure remained constant once the number of elements within the domain reached 19,251 for the only flow simulation, 12,861 for the older patient without a stent-graft simulation, 46,791 for the older patient with a stiff stent-graft simulation, and 17,266 for the older patient with a compliant stent-graft simulation.

2.2.6 Simulation Details

The governing equations along with boundary conditions and initial conditions were solved using the finite element method in COMSOL Multiphysics v5.2a (COMSOL,

Inc., Burlington, MA). The simulations were performed on a 3.4 GHz workstation with 8GB of RAM. The simulation was solved for 0.89 seconds of simulated time and the typical computation time for the simulation was two hours.

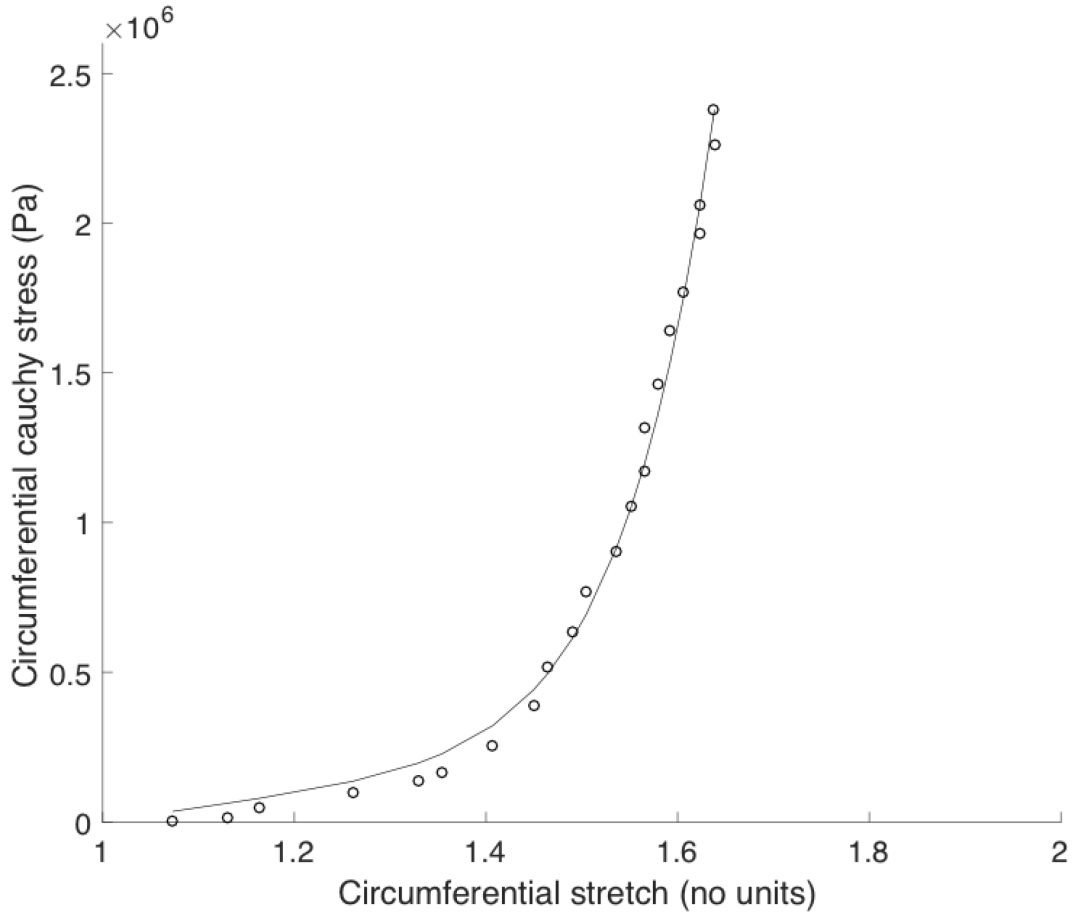

Figure 2.6: Mechanical properties of the descending thoracic aorta for an older patient (dots) and an older patient with the two-term Ogden fit (solid line). From Groenink et al., 1999 [6].

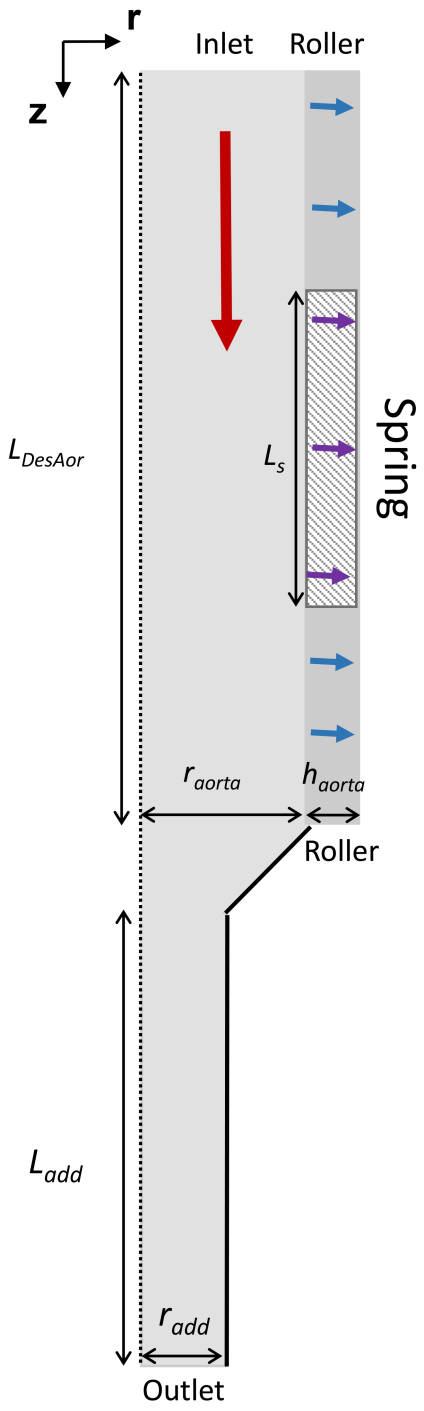

Figure 2.7: Dimensions and boundary conditions of axisymmetric COMSOL model. Description of variables in Appendix 4.

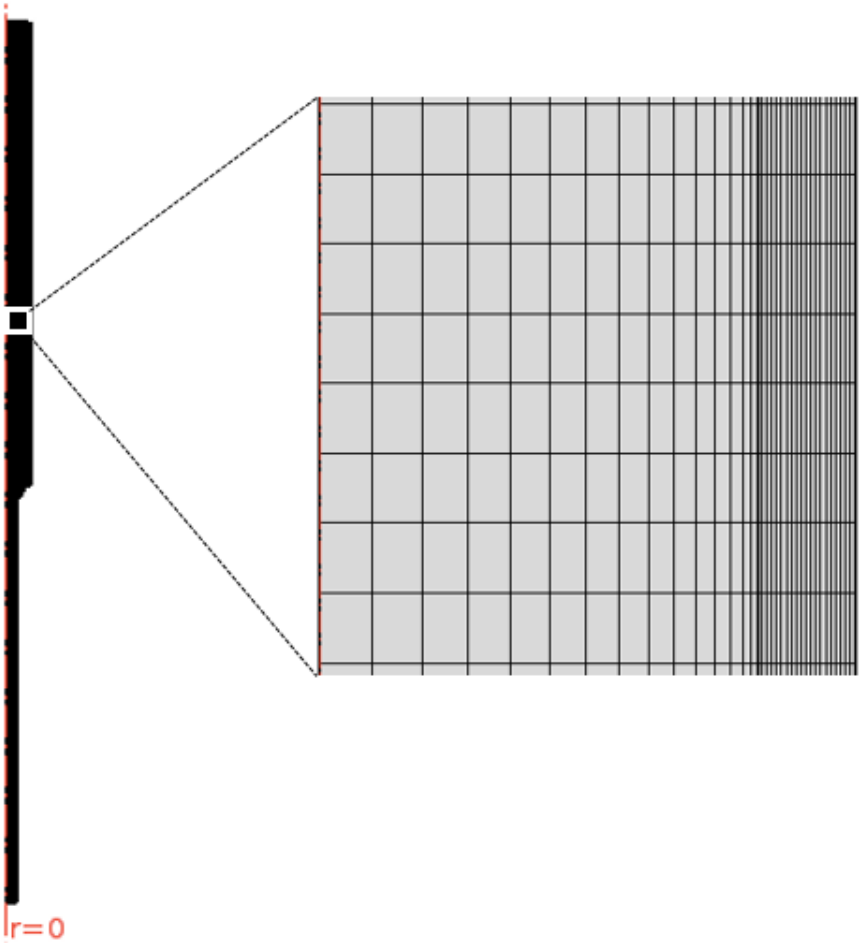

Figure 2.8: Mesh of 2D axisymmetric COMSOL model

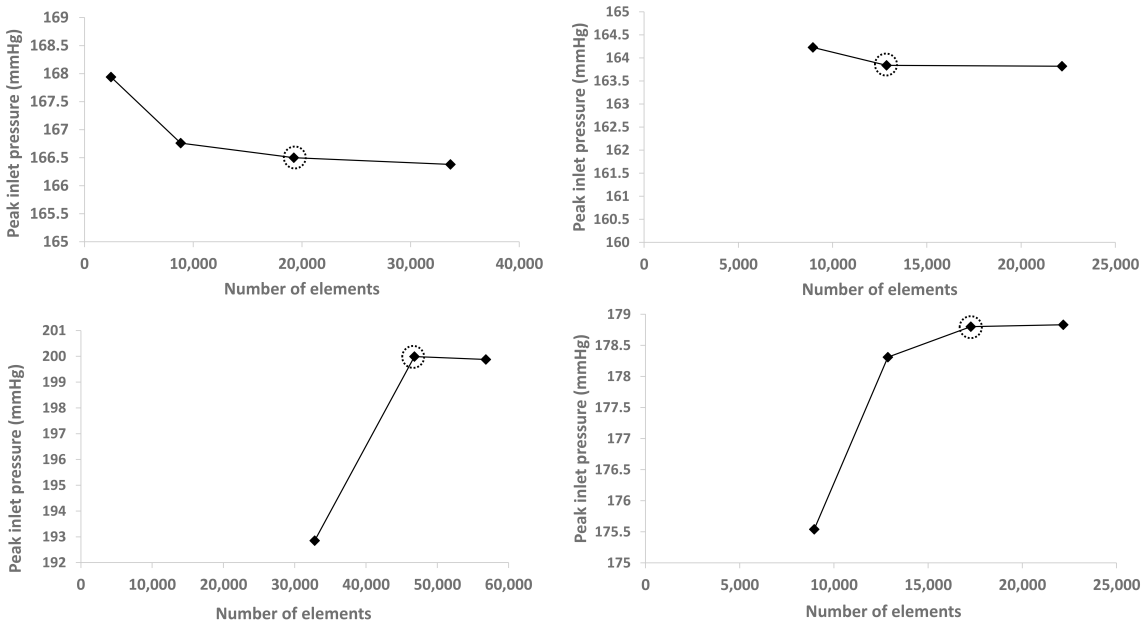

Figure 2.9: Mesh convergence of peak inlet pressure. (Top left) Only flow. (Top right) Older patient without stent-graft. (Bottom left) Older patient with stiff stent-graft. (Bottom right) Older patient with compliant stent-graft.

Chapter 3

Results

3.1 Lumped Parameter Model

Figure 3.1 shows a plot of proximal aorta pressures within the lumped parameter model for an older patient without a stent-graft, an older patient with a stiff stent-graft, and an older patient with a compliant stent-graft as a function of time. Older patients treated with a stiff stent-graft have larger maximum pressures during the length of the cardiac cycle as compared to older patients treated with a compliant stent-graft.

Figure 3.2 shows an increase in peak pressure for older aortic dissection patients treated with a longer stent-graft as compared to older aortic dissection patients treated with a shorter stent-graft.

3.2 Fluid-Structure Interaction Finite-Element Model

Figures 3.3, 3.4, 3.5, and 3.6 show a plot of the computational blood flow velocity and radial displacement in the aorta and stent-graft at the peak of the cardiac cycle for the older patient without a stent-graft, older patient with a stiff stent-graft, and older patient with a compliant stent-graft simulations. The blood flow velocity is around 1 m/s and the radial displacement in the aorta ranges between 0.3 and 0.5 mm.

Figures 3.7, 3.8, 3.9, and 3.10 shows plots of the proximal aorta pressures within

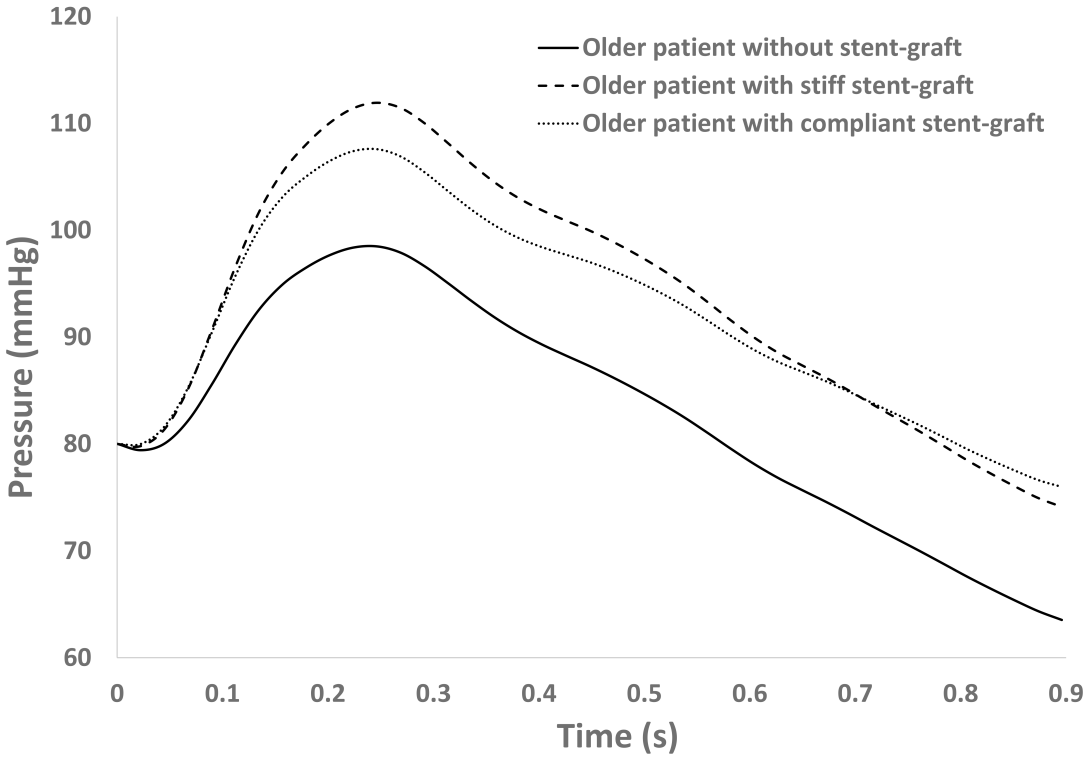

Figure 3.1: Proximal native aorta pressure using the lumped parameter model.

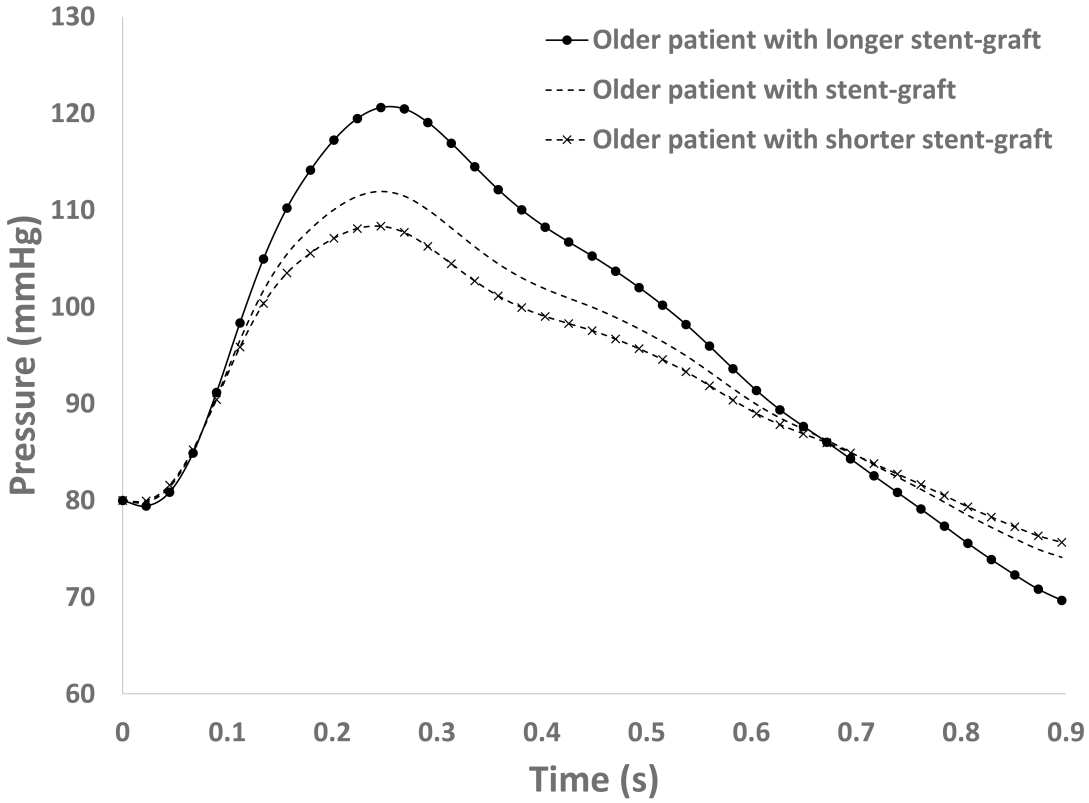

Figure 3.2: Proximal native aorta pressure using the lumped parameter model for different length stent-grafts.

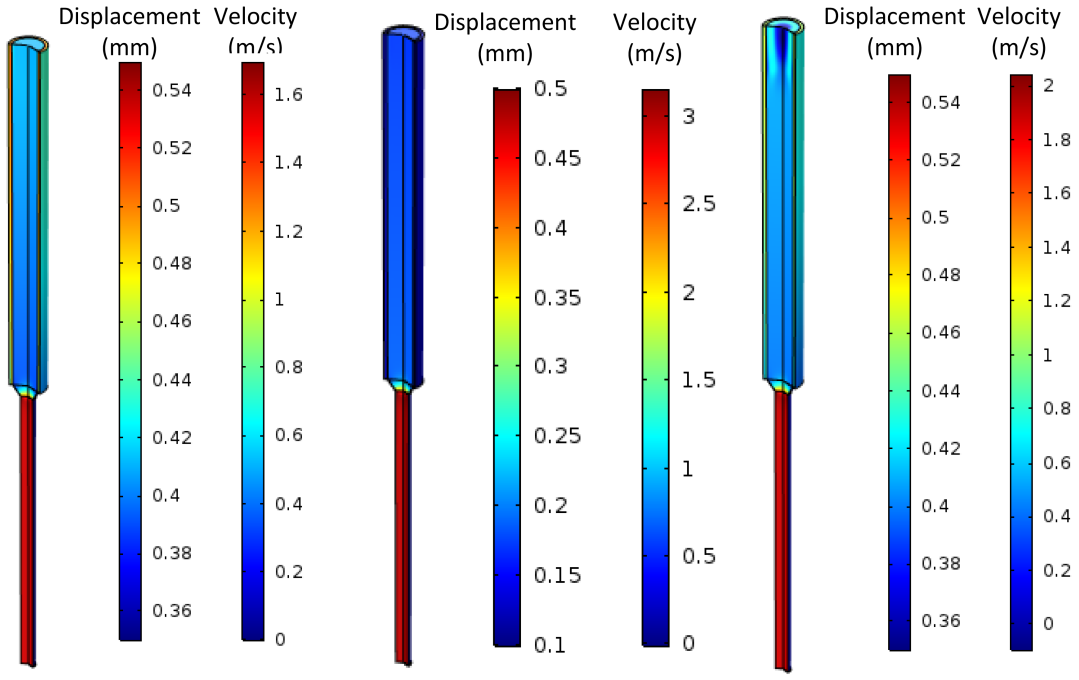

Figure 3.3: Blood velocity and aorta and stent-graft radial displacement. (Left) Older patient without stent-graft. (Middle) Older patient with 30 cm stiff stent-graft. (Right) Older patient with 30 cm compliant stent-graft.

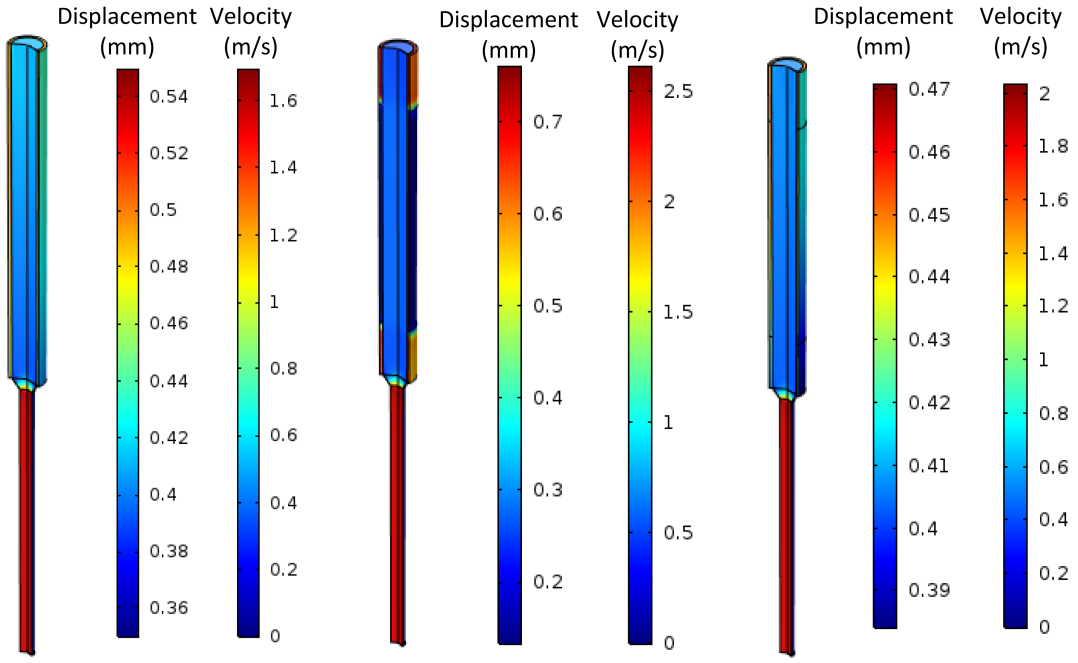

Figure 3.4: Blood velocity and aorta and stent-graft radial displacement. (Left) Older patient without stent-graft. (Middle) Older patient with 20 cm stiff stent-graft. (Right) Older patient with 20 cm compliant stent-graft.

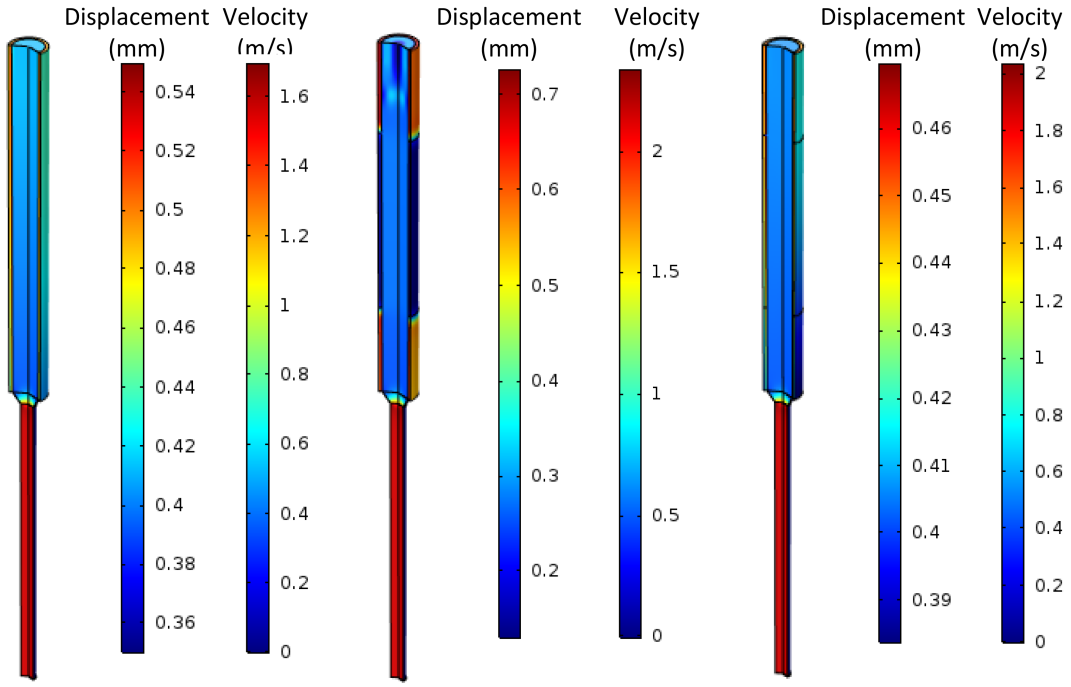

Figure 3.5: Blood velocity and aorta and stent-graft radial displacement. (Left) Older patient without stent-graft. (Middle) Older patient with 15 cm stiff stent-graft. (Right) Older patient with 15 cm compliant stent-graft.

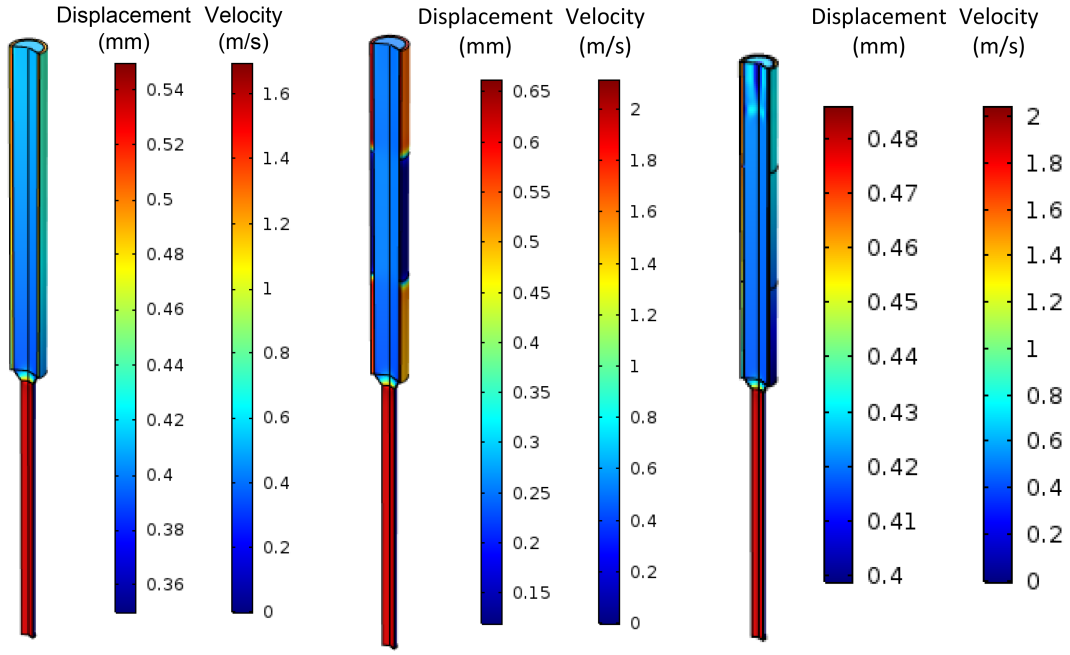

Figure 3.6: Blood velocity and aorta and stent-graft radial displacement. (Left) Older patient without stent-graft. (Middle) Older patient with 11 cm stiff-stent-graft. (Right) Older patient with 11 cm compliant stent-graft.

the transient computational model as a function of time for the older patient simulations with a 30 cm stent-graft (Figure 3.7), a 20 cm stent-graft (Figure 3.8), a 15 cm stent-graft (Figure 3.9), and an 11 cm stent-graft (Figure 3.10). Older patients treated with a stiff stent-graft have larger maximum pressures during the length of the cardiac cycle as compared to older patients treated with a compliant stent-graft. This increase in maximum pressure is exaggerated for longer stent-grafts. Table 3.2 summarizes the peak pressure over the length of the cardiac cycle for the different simulations.

Table 3.1: Peak pressure for an older patient without a stent-graft and an older patient with different length stent-grafts.

Simulation		Peak pressure [mmHg]
Older patient without a stent-graft		163.84
Older patient with 30 mm stent-graft	Stiff	199.17
	Compliant	178.31
Older patient with 20 cm stent-graft	Stiff	190.83
	Compliant	176.17
Older patient with 15 cm stent-graft	Stiff	185.72
	Compliant	176.92
Older patient with 11 cm stent-graft	Stiff	178.37
	Compliant	179.32

Validation of transient results with pulsatile flow in a rigid pipe

The phase shift between the pressure and velocity at the inlet of the descending thoracic aorta agrees well with theoretical calculations obtained from pulsatile flow in a rigid pipe.

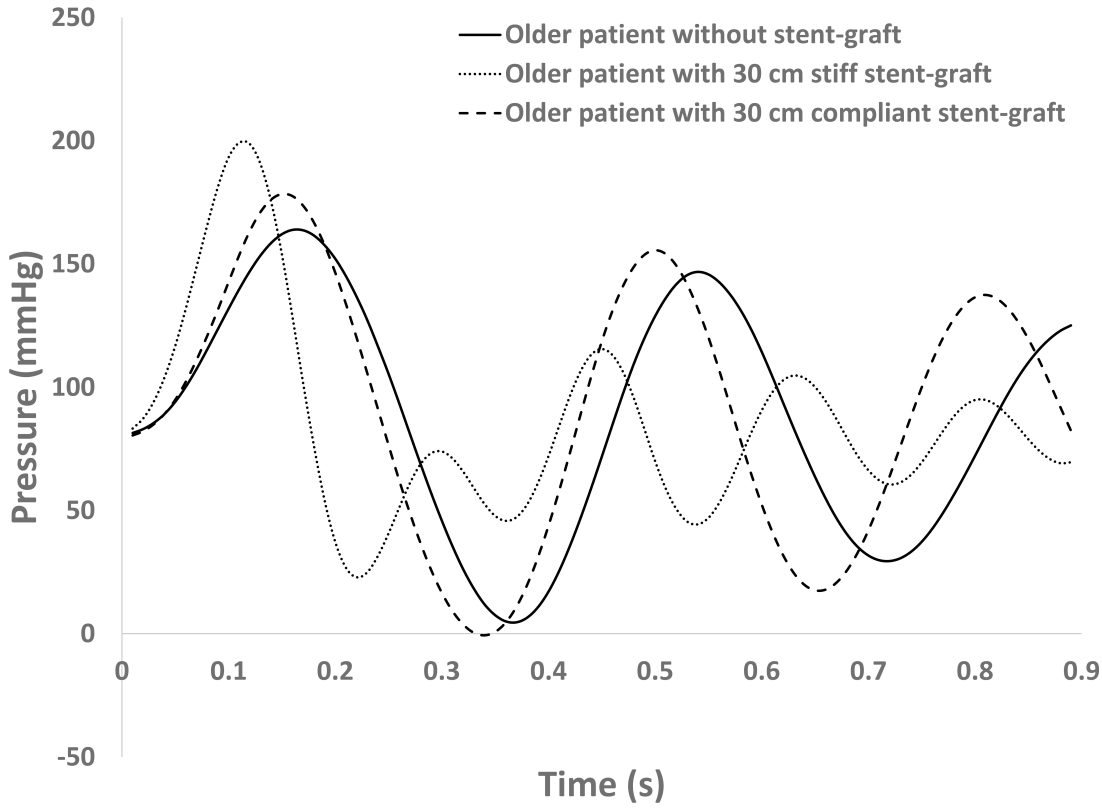

Figure 3.7: Proximal aorta pressure as a function of time in cardiac cycle for an older patient without a stent-graft, an older patient with a 30 cm stiff stent-graft, and an older patient with a 30 cm compliant stent-graft.

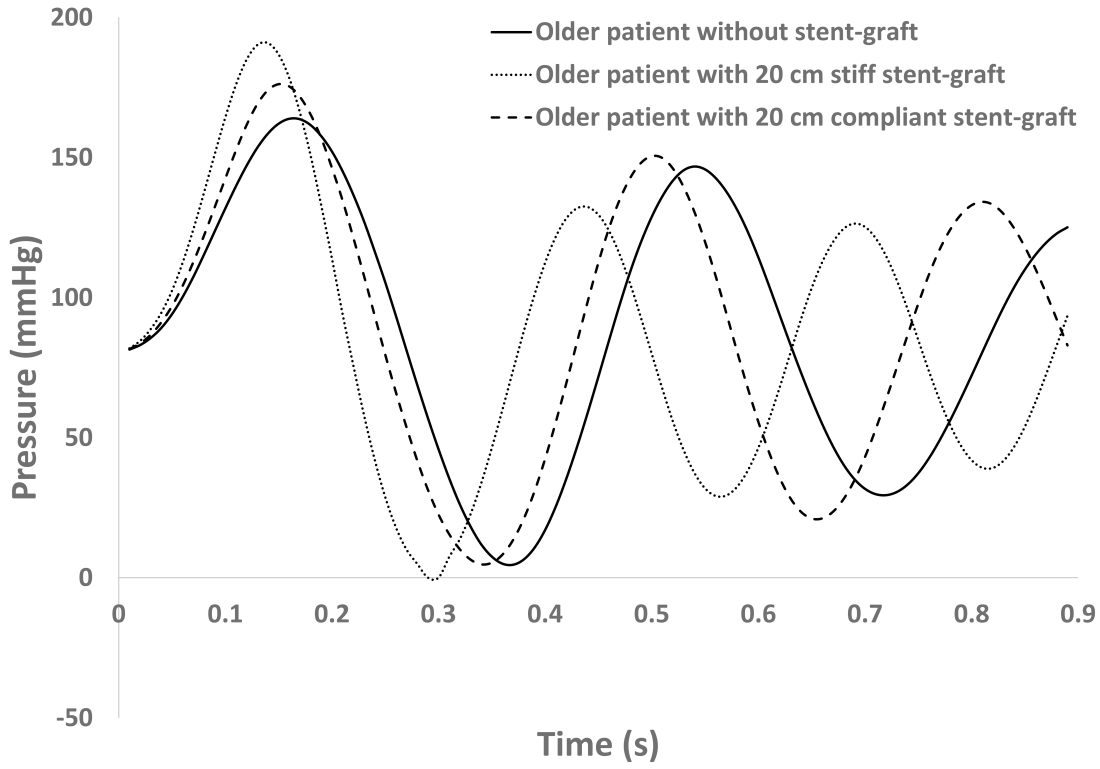

Figure 3.8: Proximal aorta pressure as a function of time in cardiac cycle for an older patient without a stent-graft, an older patient with a 20 cm stiff stent-graft, and an older patient with a 20 cm compliant stent-graft.

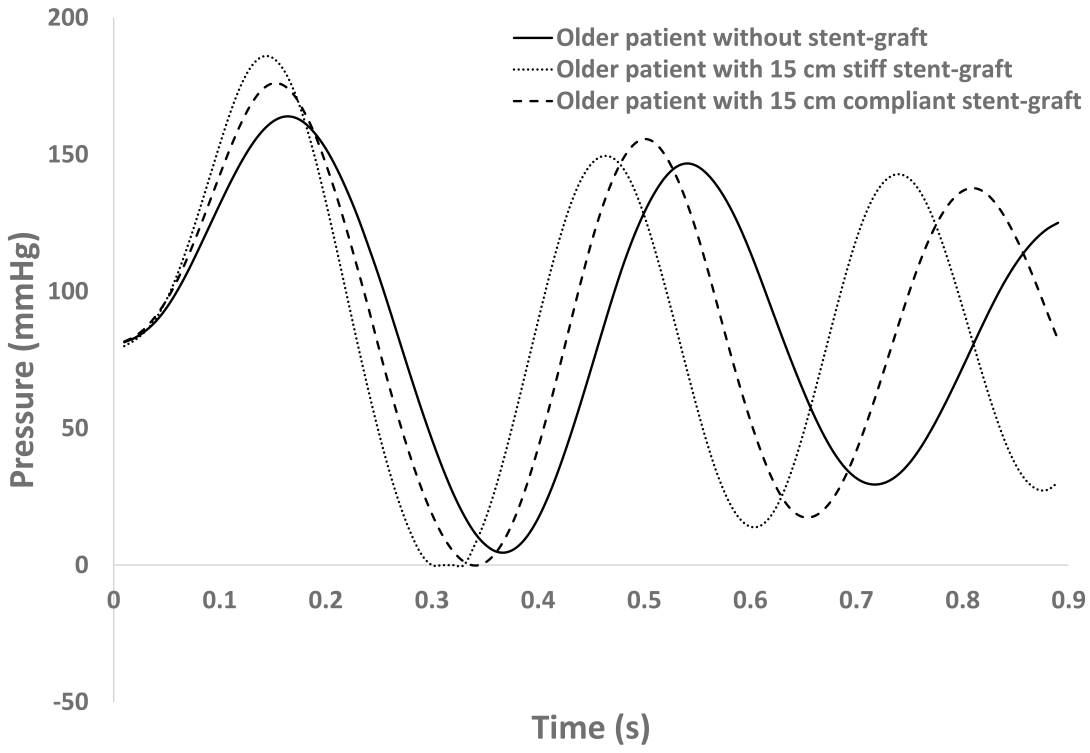

Figure 3.9: Proximal aorta pressure as a function of time in cardiac cycle for an older patient without a stent-graft, an older patient with a 15 cm stiff stent-graft, and an older patient with a 15 cm compliant stent-graft.

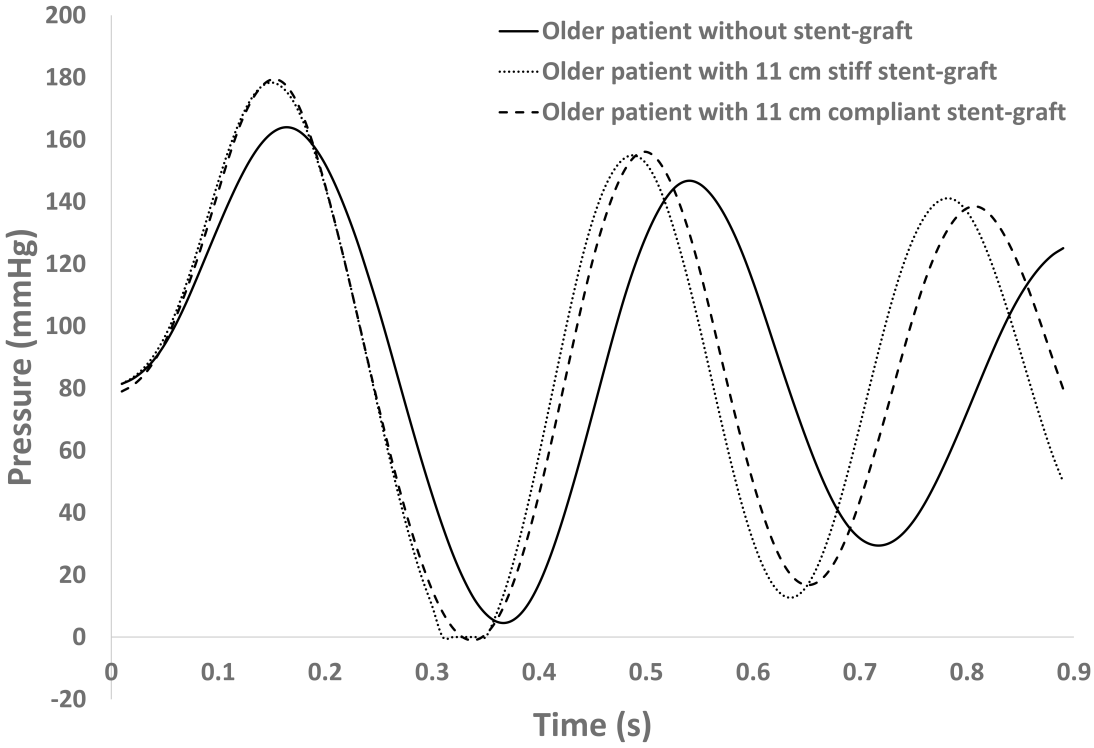

Figure 3.10: Proximal aorta pressure as a function of time in cardiac cycle for an older patient without a stent-graft, an older patient with an 11 cm stiff stent-graft, and an older patient with an 11 cm compliant stent-graft.

Table 3.2: Peak pressure for an older patient without a stent-graft and an older patient with different length stent-grafts.

Simulation		Peak pressure [mmHg]
Older patient without a stent-graft		163.84
Older patient with 30 mm stent-graft	Stiff	199.17
	Compliant	178.31
Older patient with 20 cm stent-graft	Stiff	190.83
	Compliant	176.17
Older patient with 15 cm stent-graft	Stiff	185.72
	Compliant	176.92

The velocity and pressure distributions for the laminar flow of a Newtonian fluid in a long, rigid vessel exposed to an oscillating laminar flow obey the Womersley solution according to the following derivation [17].

Blood flow is fully developed in the axial direction and therefore only the z-component of the Navier-Stokes equation in cylindrical coordinates is nonzero (Equation 3.1):

$$\rho\frac{\partial v_z}{\partial t} = -\frac{\partial P}{\partial z} + \frac{\mu}{r}\frac{\partial}{\partial r}\left(r\frac{\partial v_z}{\partial r}\right) \tag{3.1}$$

The cardiac cycle is time-periodic and therefore the pressure gradient oscillates with frequency w and can be represented as Equation 3.2:

$$-\frac{\partial P}{\partial z} = A^* e^{iwt} \tag{3.2}$$

The boundary conditions for oscillating flow through a rigid vessel are:

1. A no slip boundary condition at the wall of the vessel (Equation 3.3):

$$v_z|_{r=R} = 0 \tag{3.3}$$

2. A symmetry boundary condition at the centerline of the vessel (Equation 3.4):

$$\left.\frac{\partial v_z}{\partial r}\right|_{r=0} = 0 \tag{3.4}$$

The velocity can be represented as the product of two functions (Equation 3.5):

1. u, a function of radial position only and

2. e^{iwt}, a function of time only

$$v_z = ue^{iwt} \tag{3.5}$$

Substituting Equations 3.2, 3.5, and boundary condition Equations 3.3 and 3.4 into Equation 3.1 yields Equation 3.6.

$$\frac{-iwue^{iwt}}{v} + \frac{e^{iwt}}{r}\frac{\partial}{\partial r}\left(r\frac{\partial u}{\partial r}\right) = \frac{A^*}{\mu}e^{iwt} \tag{3.6}$$

Each term in Equation 3.6 contains the time dependent e^{iwt} term, and can be reduced to Equation 3.7.

$$\frac{\partial^2 u}{\partial r^2} + \frac{1}{r}\frac{\partial u}{\partial r} - \frac{iwu}{v} + \frac{A^*}{\mu} = 0 \tag{3.7}$$

Evaluating Equation 3.7 with the boundary conditions above, results in an equation for blood velocity as a function of time and position (Equation 3.8):

$$v_z = \frac{A^*}{iw\rho}\left(1 - \frac{J_o\left(\frac{\alpha r}{R}i^{3/2}\right)}{J_o\left(\alpha i^{3/2}\right)}\right)e^{iwt} \tag{3.8}$$

where w, is the frequency at which the velocity wave oscillates, ρ is the blood density, J_0 is the Bessel function of the first kind of order zero, r is the radial position in the vessel, R is the radius of the vessel, and α is the Womersely parameter and equals $R\sqrt{w/v}$. The Womersley number is larger in larger diameter vessels and decreases with a decrease in vessel radius. The pressure distribution within the vessel is represented as Equation 3.9:

$$P = A^* L e^{iwt} \tag{3.9}$$

The analytical input velocity is plotted as a function of time and overlaid with the computational input velocity as a function of time (Figure 3.11). The resultant analytical output pressure is plotted as a function of time and overlaid with the resultant computational output pressure as a function of time (Figure 3.12). The good agreement between the analytical and computational solutions for aorta inlet pressure, confirms that the simulation is running accurately.

Additionally, the phase shift between velocity and pressure obtained in the computational solution (Figure 3.13) agrees with the phase shift between velocity and pressure in the analytical solution (Figure 3.13). This further validates that the simulation is running accurately.

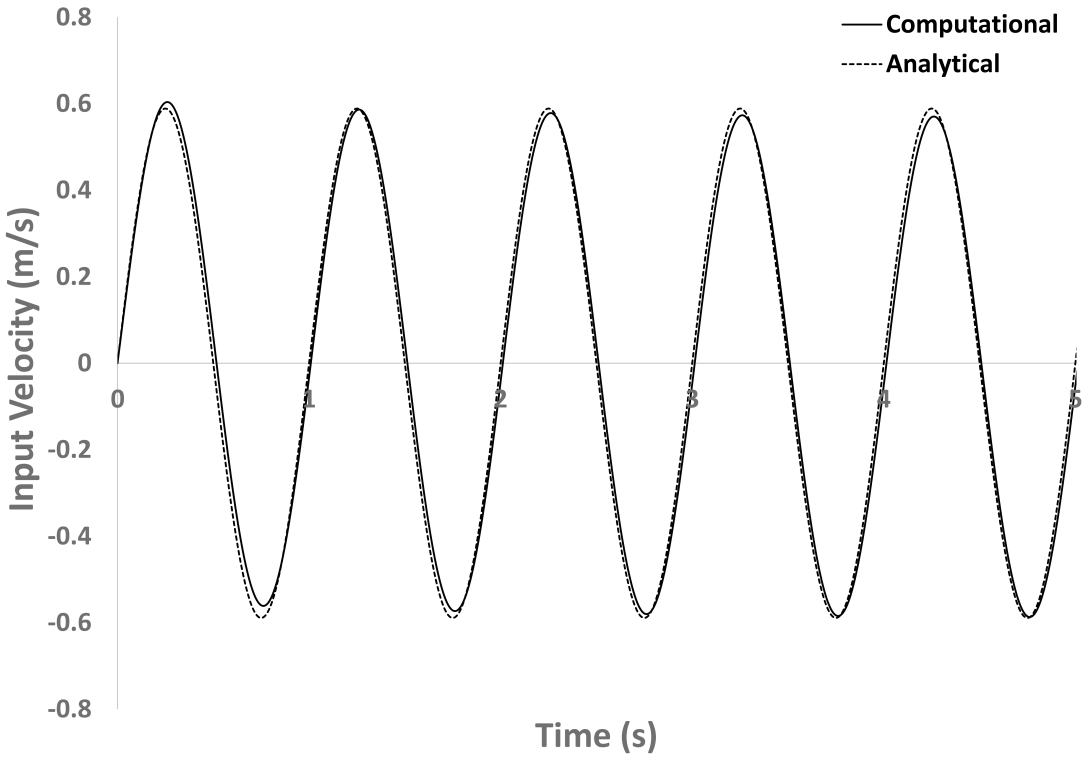

Figure 3.11: Analytical and computational input velocity for pulsatile flow in a rigid pipe.

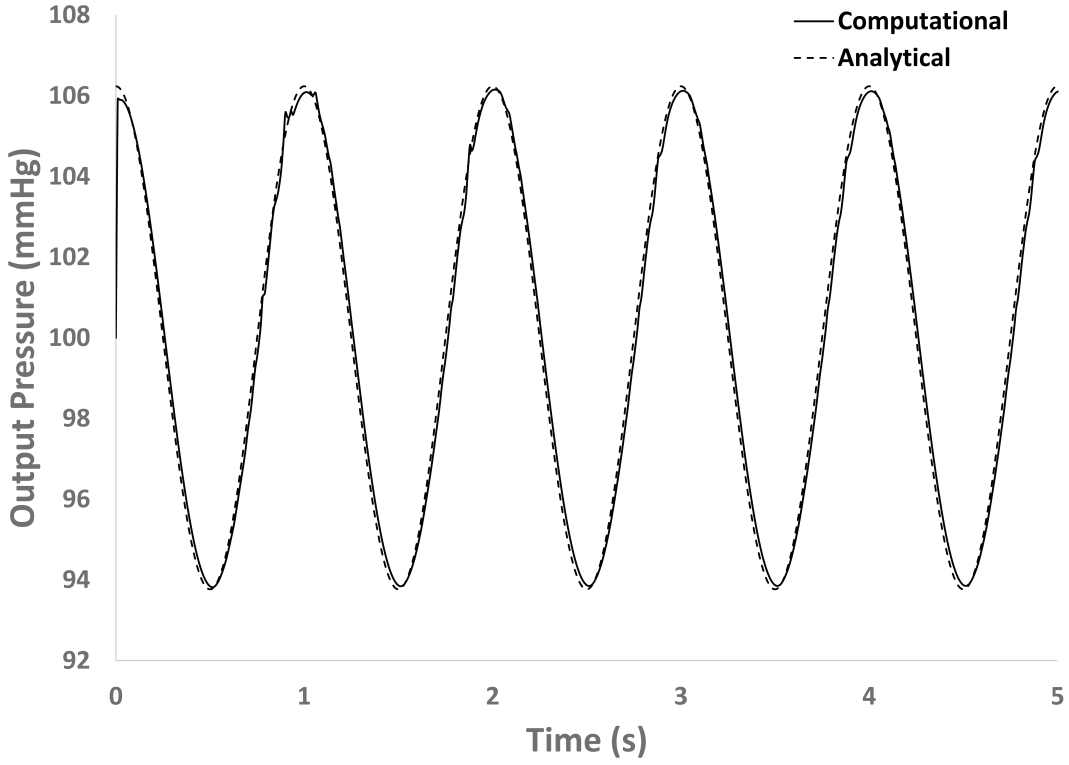

Figure 3.12: Analytical and computational output pressure for pulsatile flow in a rigid pipe.

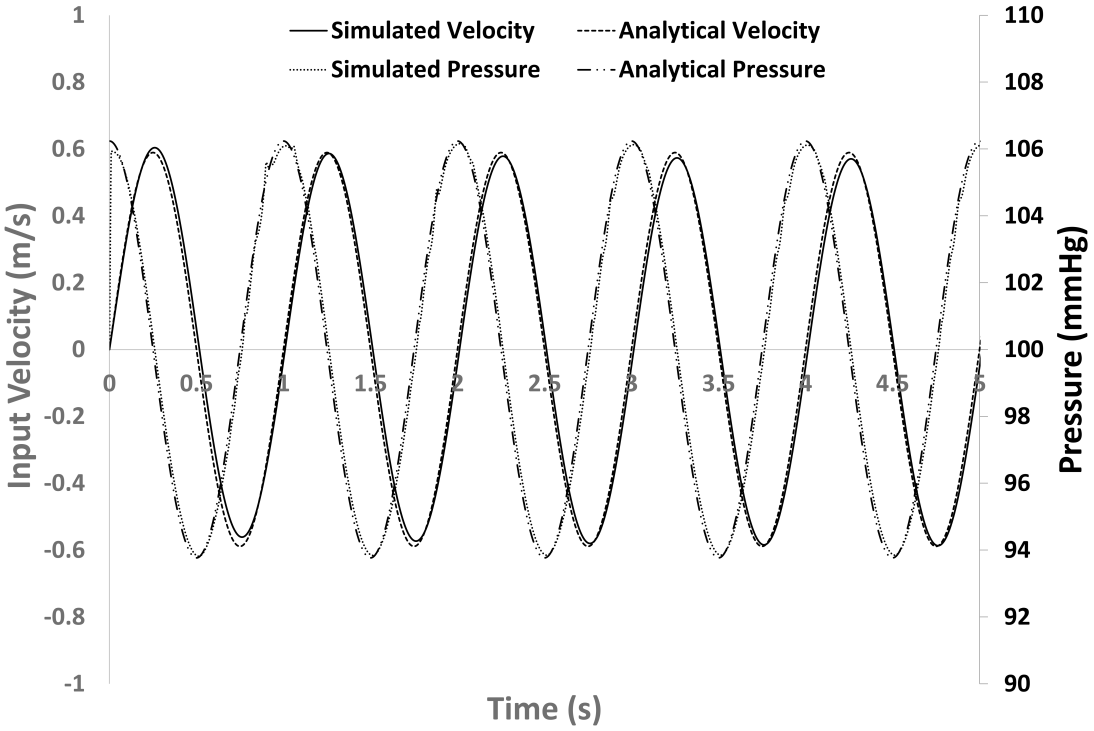

Figure 3.13: Analytical and computational phase shift between velocity and pressure in proximal aorta.

Chapter 4

Discussion

4.1 Lumped Parameter Model

The increase in pressure with the incorporation of a stiff stent-graft in the lumped parameter model can be explained using the circuit elements in relation to the windkessel model. Capacitors store charge and analogously, compliance is a mechanical construct that describes the distensibility of blood vessels. For the older patient with a stiff stent-graft, the effective compliance C_s, is smaller ($C_{s,stiff}$ = 1.224) than the older patient with a compliant stent-graft ($C_{s,compliant}$ = 1.558). According to Equation 2.4, inlet aorta pressure and aorta compliance are inversely related. Thus, the older patient with a stiff stent-graft, with a smaller effective compliance, induces a larger inlet pressure as compared to an older patient with a compliant stent-graft and larger effective compliance.

4.2 Fluid-Structure Interaction Finite-Element Model

The simulated transient pressure as a function of time can be explained using the relationship between pressure, flow rate, and vessel radius in Poiseuille flow (Equation 4.1) and the calculated pressure distribution within a vessel calculated using Womersely flow (Equation 3.9).

$$\Delta P = \frac{\mu L Q}{\pi r^4} \tag{4.1}$$

According to Equation 3.8, Equation 3.9, and Figure 3.13, there is a phase shift between the pressure and velocity at the inlet of the descending thoracic aorta, which is well-captured by our simulated data (Appendix A.5). The difference in peak pressure for the simulations of the older patient without a stent-graft and older patient with a stiff and compliant stent-graft can be explained using Poiseuille flow (Equation 4.1). For the simulation of the older patient without a stent-graft, blood interacts with the compliant vessel wall, which subsequently expands the radius of the vessel. For the simulation of the older patient with a stiff stent-graft, as blood interacts with the stiff stent-graft, there is minimal expansion of the vessel wall. Because of the inverse relationship between pressure and radius (Equation 4.2),

$$P \sim \frac{1}{r^4} \tag{4.2}$$

the older patient with stiff stent-graft, and therefore smaller vessel radius, has a higher peak pressure than the older patient with a compliant stent-graft and older patient without a stent-graft.

The induced displacement in the descending thoracic aorta is further validated with physiological data [8]. According to Humphrey, the in-vivo radial pulsation in the thoracic aorta is approximately 2.6% of the initial radius. Thus the radial displacement in our model, with a descending thoracic aorta radius of 1.25 cm should be approximately 0.325mm. The radial displacement in our model ranges between 0.3 and 0.5 mm, in good agreement with Humphrey.

4.2.1 Sensitivity Analyses on Transient Results

To understand the effect of the input parameters on the computational pressure proximal to the stent-graft, sensitivity analyses were performed by running multiple simulations for the input parameters with the highest variability.

Effect of stent-graft length on proximal aorta pressure An increase in stent-graft length increases pressures at the inlet of the descending thoracic aorta and shifts the time of peak pressure to later in the cardiac cycle (Figure 4.1). As the length of the stent-graft is increased, a larger proportion of the computational domain is stiff and cannot expand. The effective radius of the patient with a longer stent-graft is smaller than the effective radius of the patient with a shorter stent-graft. Since pressure and radius are inversely related (Equation 4.2), a longer stent-graft, and thus smaller effective radius indicates a larger peak pressure.

As expected, Table 3.2, shows an increase in stent-graft length increases the peak pressure of the cardiac cycle.

Effect of stent-graft modulus on proximal aorta pressure A change in stent-graft modulus has minimal effect on the pressure at the inlet of the descending thoracic aorta (Figure 4.2). The effective radius of the vessel in the simulations with different moduli are the same and thus the peak pressure is also the same. Only with a significant decrease in stent-graft modulus (so as to match the compliance of the native aorta) is there an effect on the pressure proximal to the location of the stent-graft (Figure 4.2).

Effect of stent-graft location on proximal aorta pressure A translation in stent-graft location has no effect on the pressure at the inlet of the descending thoracic aorta (Figure 4.3). The length of the stent-graft remains unchanged in the different simulations, therefore the effective radius of the vessel with different stent-graft positions are the same. Thus, the maximum pressure during the length of the cardiac cycle is unaffected by a translation of the stent-graft.

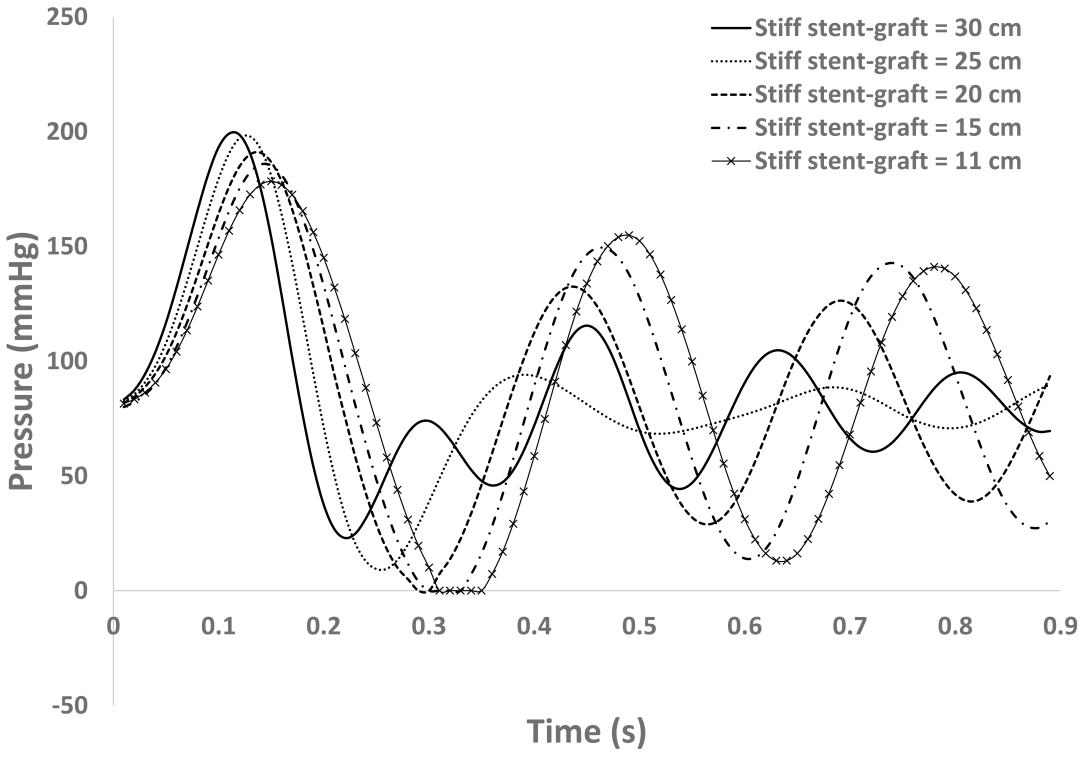

Figure 4.1: Stent-graft length sweep, stent-graft modulus = 5MPa

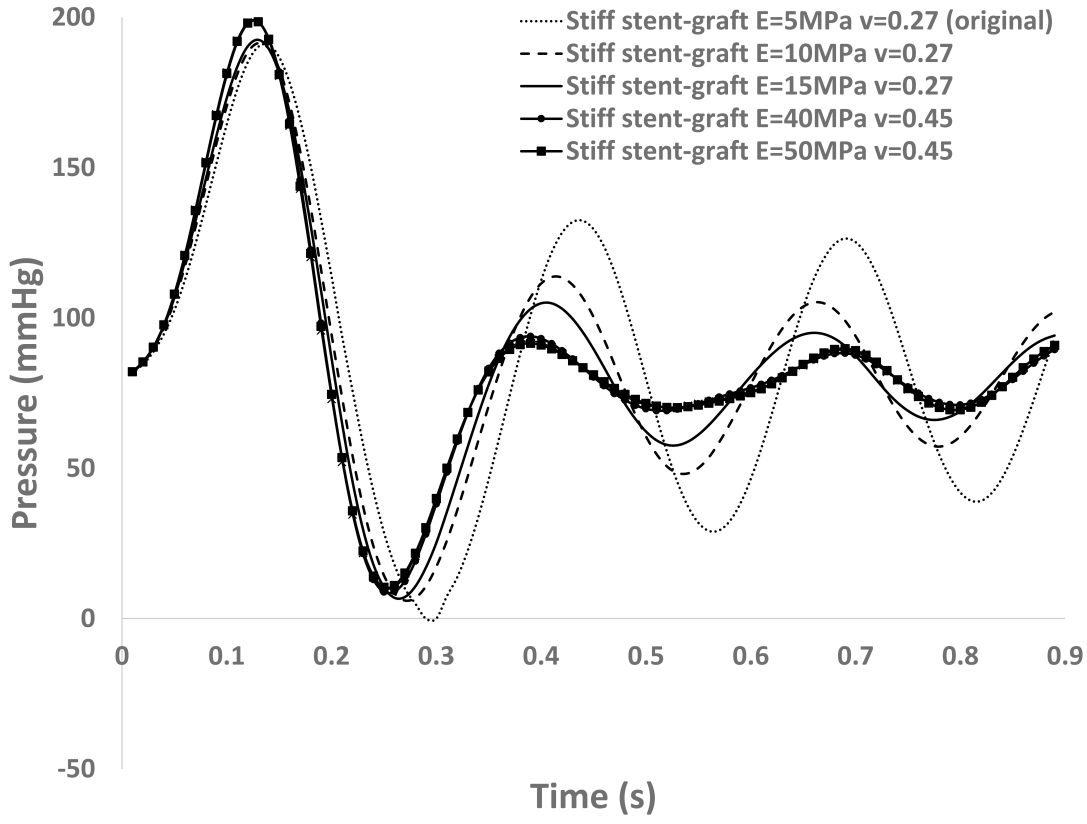

Figure 4.2: Stent-graft modulus sweep, stent-graft length = 20 cm.

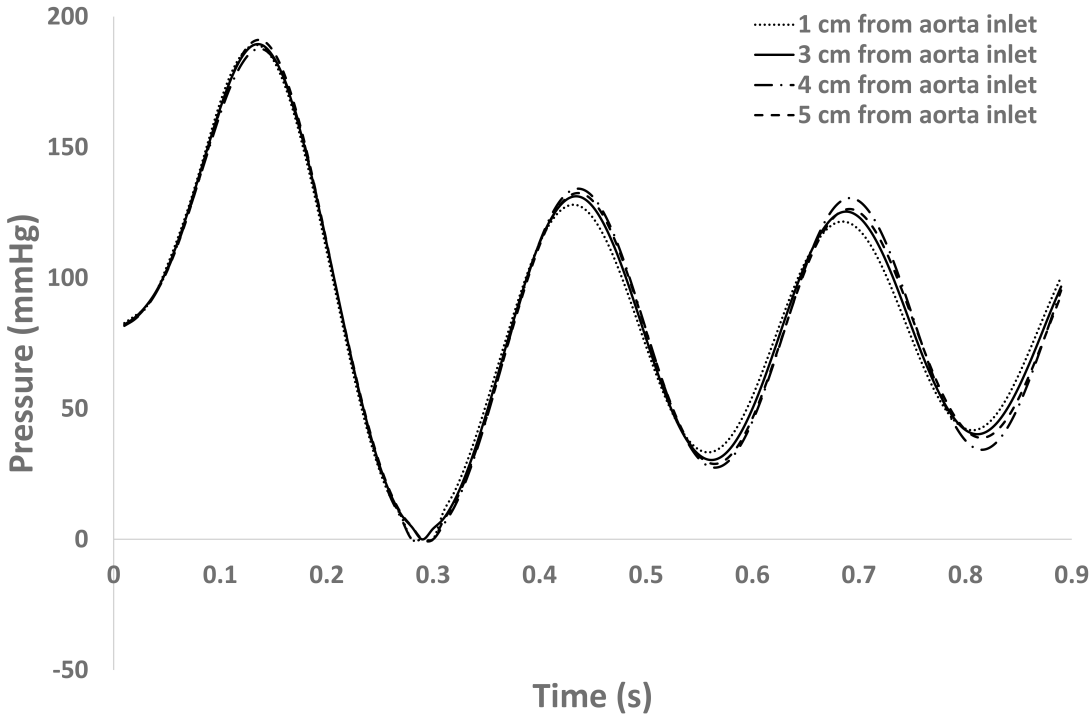

Figure 4.3: Stent-graft position sweep, stent-graft length = 20 cm

Chapter 5

Conclusion

The objective of this work was to investigate whether one fundamental cause of SINE dissections is an increase in blood pressure with the incorporation of a stiff stent-graft into the native aorta.

The lumped parameter simulation shows that the pressure at the inlet of the descending thoracic aorta, proximal to the stent-graft, is increased with the incorporation of a rigid stent-graft within the native aorta. The inlet pressures are reduced with the incorporation of a compliant stent-graft within the native aorta. This validates our hypothesis using the lumped parameter model, that the incorporation of a compliant stent-graft reduces pressure proximal to the stent-graft in the descending thoracic aorta and could limit the risk of SINE dissections.

The three-dimensional computational simulation shows an increase in proximal pressure for aortic dissection patients treated with a stiff stent-graft as compared to aortic dissection patients treated with a compliant stent-graft. This further validates our hypothesis that the incorporation of a compliant stent-graft reduces pressure proximal to the stent-graft and could limit the risk of stent-graft induced new tears.

The lumped parameter and computational models developed in this thesis serve to explore the coupling between blood flow amd aortic and stent-graft displacement. The results confirm that the stiffness of the stent-grafts used to treat aortic dissection affects blood pressure in the proximal native aorta and could contribute to the formation of

stent-graft induced new tears. This information is critical to the development of future stent-grafts to treat aortic dissection.

5.1 Limitations and Future Work

The present work is limited to evaluating the effect of a stiff stent-graft on proximal aorta pressures in a lumped parameter mathematical model and a computational model using a simplified three-dimensional geometry of the descending thoracic aorta. It would be valuable to the scientific community to model the flow and resulting aortic and stent-graft deformation using an anatomically accurate geometry of the descending thoracic aorta.

In the current model, the resistance of the peripheral vasculature is artificially incorporated into the computational domain by use of a domain added to the domain of the descending thoracic aorta. This is added to allow pressures within the descending thoracic aorta to build up physiologically and allow for the appropriate physiological displacement in the aortic material. Cardiovascular flow simulation packages like SimVascular, may be able to capture this boundary condition without the incorporation of an artificial domain [22].

The model developed in this study is valuable in evaluating the impact of blood flow through a stiff and compliant stent-graft on the overall native aorta proximal pressures.

Chapter 6

Bibliography

[1] AlKhaderi, Sakher. "IMAGING OF AORTIC DISSECTION." YouTube. YouTube, 12 Jan. 2016. Web. 09 Mar. 2017. ⟨https://www.youtube.com/watch?v=kEuwyMekLM⟩ .

[2] "Aortic Dissection." Sayed Feghali Cardiology Association. Little Grey Bike, n.d. Web 08 Mar. 2017. ⟨http://feghalicardiology.com/aortic-dissection/⟩.

[3] Brunkwall J, Kasprzak P, Verhoeven E, Heijmen R, Yalor P: "Endovascular Repair of Acute Uncomplicated Aortic Type B Dissection Promotes Aortic Remodelling: 1 Year Results of the ADSORB Trial." *European Journal of Vascular and Endovascular Surgery*, **48**: 285-291, 2014.

[4] Degroote, J. *Development of Algorithms for the Partitioned Simulation of Strongly Coupled Fluid-Structure Interaction Problems.* Ph.D Dissertation, Universiteit Gent, 2010.

[5] Dotter C, Roberts D, Steinberg I : "Aortic Length: Angiocardiographic Measurements." *Circulation*, **11**: 915-920, 1950.

[6] Groenink M, Langerak S, Vanbavel E, van der Wall E, Mulder B, can der Wal A, Spaan J: "The influence of aging and aortic stiffness on permanent dilation and

breaking stress of the thoracic descending aorta." *Cardiovascular Research,* **42**: 471-480, 1999.

[7] Hansen, M.S. *Boundary Conditions for 3D Fluid- Structure Interaction Simulations of Compliant Vessels.* Masters Thesis, Norwegian University of Science and Technology, 2013.

[8] Humphrey, J. D. (2002). *Cardiovascular solid mechanics: Cells, tissues, and organs.* New York: Springer.

[9] Juang D, Braverman A, Eagle K: "Aortic Dissection." *Circulation,* **118**: 507-510, 2008.

[10] Kind T, Faes T, Lankhaar JW, Vonk-Noordegraaf A, Verhaegen M: "Estimation of Three- and Four-Element Windkessel Parameters using Subspace Model Identification." *IEEE Transactions on Biomedical Engineering*, **57**:7, 2010.

[11] Kleinstreuer, C. (2006) *Biofluid Dynamics: Principles and Selected Applications.* Boca Raton, FL: Taylor & Francis.

[12] Kousera C, Wood N, Seed, W, Torii R, ORegan D, Xu, X: "A Numerical Study of Aortic Flow Stability and Comparison with In Vivo Flow Measurements." *Journal of Biomechanical Engineering*, **135**: 1-8; 2013.

[13] Kruger T, Veseli K, Lausberg H, Vohringer L, Schneider W, Schlensak C: "Regional and directional compliance of the healthy aorta: an ex vivo study in a porcine model." *Interactive Cardiovascular Thoracic Surgery*, **23**:104-111, 2016.

[14] Lantz J, Renner J, Karlsson M: "Wall shear stress in a subject specific human aorta- influence of fluid-structure interaction." *International Journal of Applied Mechanics,* 2011.

[15] LeMaire S, Russell L: "Epidemiology of thoracic aortic dissection." *Nature Review Cardiology*, **8**: 103-113, 2011.

[16] Nienaber C, Eagle K: "Aortic Dissection: New Frontiers in Diagnosis and Management, Part II: Therapeutic Management and follow-up." *Circulation,* **108**: 772-778, 2003.

[17] Pantaleo A, Jafrancecso G, Buia F, Leone A, Lovato L, Russo V, Di Marco L, Bartolomeo R, Pacini D: "Distal Stent Graft-Induced New Entry: An Emerging Complication of Endovascular Treatment in Aortic Dissection." *The Annals of Thoracic Surgery*, **102**:527-532, 2016.

[18] Roy D, Kauffman C, Delorme S, Lerouge S, Cloutier G, Soulez G: "A Literature Review of the Numerical Analysis of Abdominal Aortic Aneurysms Treated with Endovascular Stent Grafts." *Computational and Mathematical Methods in Medicine*, **2012**, Article ID 820389, 16 pages, 2012.

[19] Steinman, D. Variability of Computational Fluid Dynamics Solutions for Pressure and Flow in a Giant Aneurysm: "The ASME 2012 Summer Bioengineering Conference CFD Challenge." *Journal of Biomechanical Engineering*, **135**(2), 2013.

[20] Shier, D, Jackie, B, and Ricki, L (2010). *Hole's Human Anatomy & Physiology.* Dubuque: McGraw-Hill.

[21] Truskey G A , Yuan F, and Katz D (2004). *Transport Phenomena in Biological Systems.* Upper Saddle River, NJ: Pearson/Prentice Hall.

[22] Updegrove, A., Wilson, N., Merkow, J., Lan, H., Marsden, A. L. and Shadden, S. C., SimVascular - An open source pipeline for cardiovascular simulation, Annals of Biomedical Engineering (2016). DOI:10.1007/s10439-016-1762-8 (2016)

[23] Westerhof N, Lankhaar J, Westerhof, B: "The arterial Windkessel." *Medical and Biological Engineering and Computing,* **47**:131-141, 2009.

Appendix A

A.1 Nomenclature

Symbol

C	Compliance of aorta, mL/mmHg
C_1	Compliance of native aorta, mL/mmHg
C_2	Compliance of stent-graft, mL/mmHg
C_3	Compliance of native aorta, mL/mmHg
C_s	Effective compliance of native aorta and stent-graft in series, mL/mmHg
E	Young's modulus, Pa
h	Thickness, mm
I	Current, Amp
J_0	Bessel function of the first kind of order zero
k	Spring constant per unit area, $\mathrm{N/mm^2}$
L	Length, cm
P	Pressure, mmHg
Q	Flow rate, $\mathrm{m^3/s}$
r	Radius, cm
R	Radius of vessel
R_{es}	Resistance, Ohms and $\mathrm{Pa \cdot s/m^3}$
R_{tot}	Total peripheral resistance, $\mathrm{mmHg \cdot s/mL}$
t	Time, s

	u	Displacement of solid, m
	v	Velocity, m/s
	V	Voltage, Volts
	W	Strain energy density function
	Z	Impedance of proximal aorta, mmHg $\cdot$ s/mL
Greek		
	α	Womersley parameter
	α_1	Ogden fitting parameter
	α_2	Ogden fitting parameter
	ϵ	Strain
	λ_1	Principal stretch in 1 direction
	λ_2	Principal stretch in 2 direction
	λ_3	Principal stretch in 3 direction
	μ	Viscosity, Pa $\cdot$ s
	μ_1	Ogden fitting parameter, Pa
	μ_2	Ogden fitting parameter, Pa
	ν	Poisson's ratio
	ω	Frequency, Hz
	ρ	Density, kg/m^3
	σ	Cauchy stress, N/m^2
Subscripts		
	add	Additional region to account for resistance of peripheral vasculature
	aorta	Aorta material
	blood	Blood material
	min	Minimum
	s	Spring
	solid	Aorta and stent-graft material
	stent	Stent-graft material
	tissue	Tissue and organs surrounding aorta

A.2 Physiological values for blood flow rate into aorta

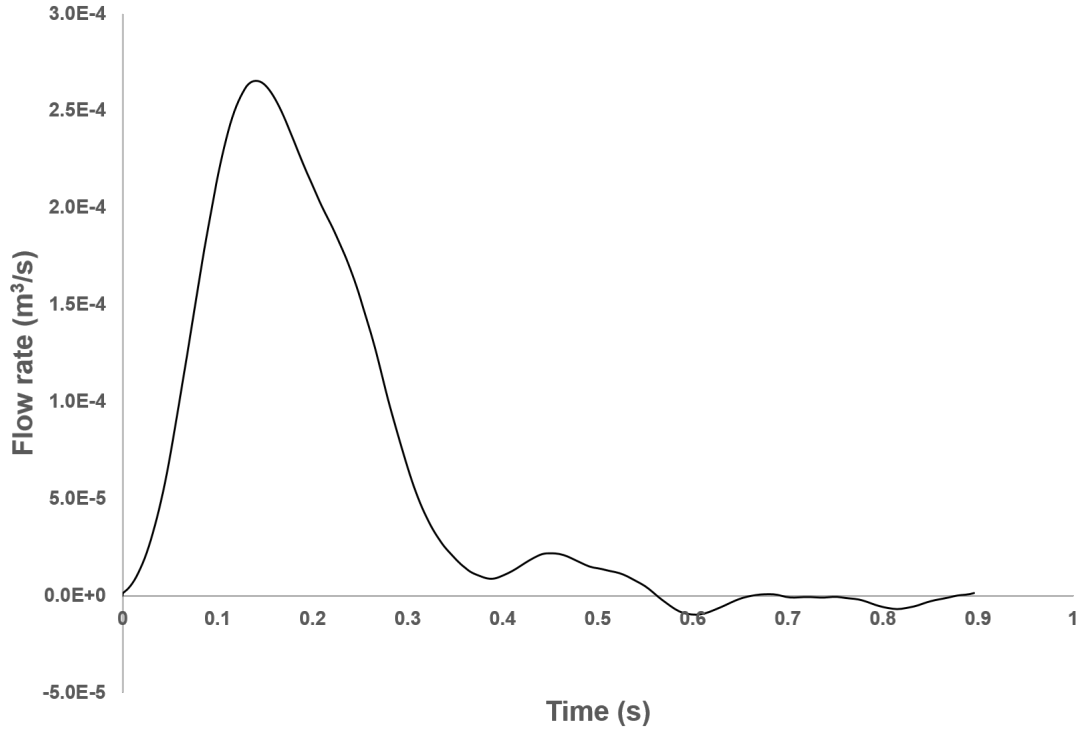

Figure A.1: Physiological values for the flow rate of blood into the aorta [12].

The physiological flow rate of Figure A.1 is decomposed by Fourier transform for easier analysis (Equation A.1).

$$\begin{aligned} Q(t) = a_0 + a_1 cos(wt) + b_1 sin(wt) + \\ a_2 cos(2wt) + b_2 sin(2wt) + a_3 cos(2wt) + b_3 sin(3wt) + \\ a_4 cos(4wt) + b_4 sin(4wt) + a_5 cos(5wt) + b_5 sin(5wt) + \\ a_6 cos(6wt) + b_6 sin(6wt) + a_7 cos(7wt) + b_7 sin(7wt) + \\ a_8 cos(8wt) + b_8 sin(8wt) \end{aligned} \tag{A.1}$$

Table A.2: Constants for Fourier Transform of physiological flow rate data

Constant	Value	Constant	Value
a_0	57.79	b_1	92.9
a_1	30.38	b_2	48.18
a_2	41.14	b_3	-6.41
a_3	-35.98	b_4	-5.29
a_4	-6.888	b_5	-7.65
a_5	-5.89	b_6	-6.8
a_6	0.172	b_7	-1.76
a_7	2.814	b_8	-0.3402
a_8	1.812	w	7.021

A.3 Constants for circuit elements

Table A.3: Constants of circuit elements in lumped parameter model

Simulation	Z	R_{tot}	C_1	C_2	C_3
Older patient with stiff stent-graft	0.05	1.4	4.5	2.1	4.5
Older patient without stent-graft	0.033	0.95	4.5	4.5	4.5
Older patient with compliant stent-graft	0.05	1.4	4.5	3.3	4.5

A.4 Model input parameters

Table A.4: Input parameters for COMSOL model

Parameter	Description	Value	Source
E_{stent} (MPa)	Young's modulus of stent-graft	5	5
h_{aorta} (mm)	Thickness of aorta wall	2.8	5
k_{tissue} (N/mm^2)	Spring constant per unit area	9,997,500	14
L_{add} (cm)	Length of additional domain	26	-
L_{DesAor} (cm)	Length of descending thoracic aorta	30	5
L_{stent} (cm)	Length of stent-graft	11-30	18
μ_{blood} (Pa $\cdot$ s)	Dynamic viscosity of blood	0.00256	14
v_{aorta}	Poisson's ratio of aorta	0.499	14
v_{stent}	Poisson's ratio of stent-graft	0.27	18
P_{min} (mmHg)	Minimum pressure of cardiac cycle	80	-
r_{add} (cm)	Radius of additional domain	6.25	-
r_{aorta} (cm)	Radius of aorta, blood domain	12.5	5
ρ_{aorta} (kg/m^3)	Density of aorta	1,080	14
ρ_{blood} (kg/m^3)	Density of blood	1,080	14
ρ_{stent} (kg/m^3)	Density of stent-graft	6,450	18

A.5 Simulation Check

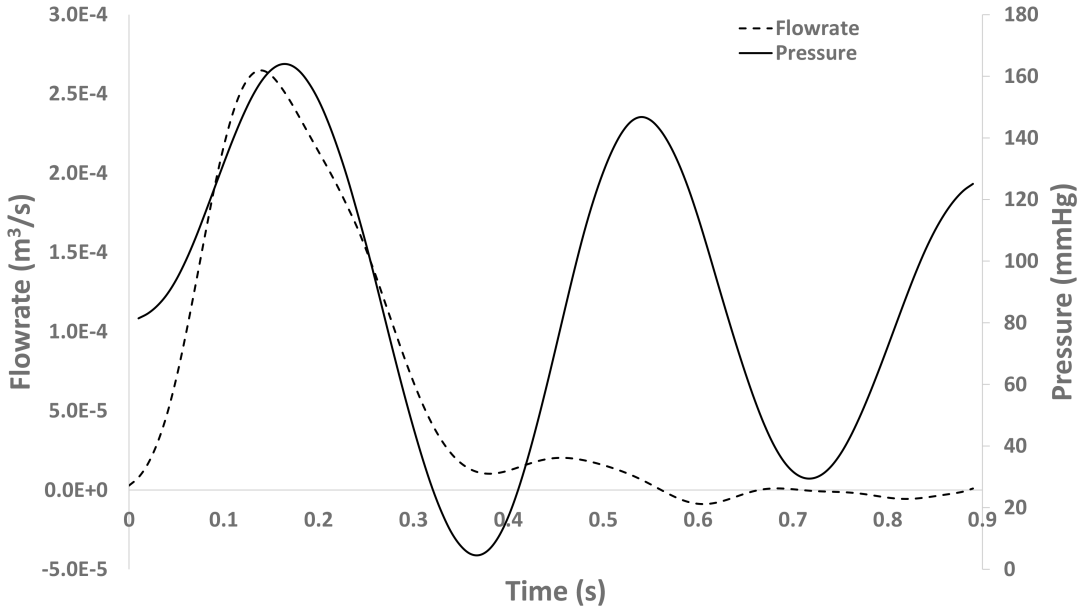

Figure A.2: Pressure and flow rate at the inlet of the descending thoracic aorta for an older patient without a stent-graft.